AFOSR TR 97-0632

REPORT DOCUMENTATION PAGE

Form Approved
OMB No. 0704-0188

1. AGENCY USE ONLY *(Leave blank)*	2. REPORT DATE	3. REPORT TYPE AND DATES COVERED
	November 1997	Final: August 1996-August 1997

4. TITLE AND SUBTITLE
Corrosion of Metal Matrix Composites

5. FUNDING NUMBERS
G-F49620-93-1-0500
P-3484/AS

6. AUTHOR(S)
Ian W. Hall

7. PERFORMING ORGANIZATION NAMES(S) AND ADDRESS(ES)
Department of Mechanical Engineering and
Department of Mathematical Sciences
University of Delaware
Newark, DE 19716

8. PERFORMING ORGANIZATION REPORT NUMBER
N/A

9. SPONSORING / MONITORING AGENCY NAMES(S) AND ADDRESS(ES)
AFOSR/NA
110 Duncan Avenue, Room B115
Bolling AFB, DC 20332-8080

10. SPONSORING / MONITORING AGENCY REPORT NUMBER

11. SUPPLEMENTARY NOTES
N/A

19971203 155

a. DISTRIBUTION / AVAILABILITY STATEMENT
Unlimited

DISTRIBUTION STATEMENT A
Approved for public release;
Distribution Unlimited

12. DISTRIBUTION CODE

13. ABSTRACT *(Maximum 200 words)*

Long term immersion testing and short term electrochemical testing have been carried out on two metal matrix composites and their corresponding unreinforced alloys. The composites were 15%alumina reinforced 6061-Al alloy and an Al-Si alloy reinforced with 20, 30, 40 or 55% SiC particles. It is shown that the pitting potentials are essentially independent of the presence or absence of reinforcement particles, as well as of their volume fraction. Corrosion i shown to be generally more severe in the composites than in the unreinforced alloy and weight loss rates may be 3 or 4 times greater. The presence of intermetallic particles strongly affects the corrosion and titanium/zirconium-rich particles, believed to arise as a consequence of the processing route, have been shown to have a particularly deleterious effect on corrosion of the 6061-Al alloy.

14. SUBJECT TERMS	15. NUMBER OF PAGES
Corrosion, pitting, metal matrix composite, alumina, silicon carbide, aluminum	41
	16. PRICE CODE

17. SECURITY CLASSIFICATION OF REPORT	18. SECURITY CLASSIFICATION OF THIS PAGE	19. SECURITY CLASSIFICATION OF ABSTRACT	20. LIMITATION OF ABSTRACT
UNCLASSIFIED	UNCLASSIFIED	UNCLASSIFIED	UL

"Corrosion of Metal Matrix Composites"

Ian W. Hall

Department of Mechanical Engineering
and
Department of Mathematical Sciences
University of Delaware
Newark, DE 19716

Final Report
Grant # F49620-93-1-0500
Air Force Office of Scientific Research
Bolling AFB, DC 20332-8080

November 1997

1. Introduction

This report concerns primarily the results of a one year no-cost extension to AFOSR Award Number F49620-93-1-0500, entitled "Non-Destructive Evaluation of Corrosion Damaged Structures". The principal focus of the award was the evaluation of a method for non-destructive examination of metallic structures based upon the proposed method of electrical impedance tomography, an analytical study of the electrical impedance tomography problem and development of efficient algorithms for its application to imaging cracks in real structures. A secondary goal was the application of the method to actual and potential future aircraft alloys and generation of fundamental data concerning their corrosion behavior. The materials proposed for study were metal matrix composites which are being increasingly used in advanced engineering applications but for which relatively little information concerning their corrosion behavior was available.

The major portion of the research concerning the analysis of the electrical impedance tomography (EIT) method was completed and reported last year [1] by the Principal Investigator Prof. F. Santosa, now at the University of Minnesota. The research on corrosion of metal matrix composites has now been completed at the University of Delaware under Prof. I. W. Hall as Principal Investigator. The present report is, therefore, divided into two sections. The first section will briefly summarize the results of the EIT analytical portion of the research and the second section will present the results of the extensive investigation of corrosion phenomena in metal matrix composites.

Section 1
"Electrical Impedance Tomography"

1.1 Introduction

Nondestructive flaw detection is a central priority for the current efforts involved in assuring the integrity of aging aircraft [2]. This section of the report concerns initial efforts to apply a computer assisted electrostatic method to the problem of crack detection in alloys. Briefly, this technique consists of passing a steady electric current through the sample and monitoring the potential at a series of locations on the specimen with an array of probes. Specifically, we collect voltage potential drop as a function of position within a part of the sample. Uniform samples show correspondingly uniform potential drops while defective samples show irregularities in the potential field. Deconvolution of the measured signals should allow details of the shape, location, and size of the defect to be determined. A major advantage of the system is that probes applied to the front surface of the sample can be used to reveal defects on the rear surface, allowing the detection of cracks and discontinuities on interior or hidden surfaces.

Prior work has confirmed [3,4] that the technique is capable of detecting surface irregularities occurring on one side of a thin plate by monitoring potential drops on the other (accessible) side of the plate. By analyzing the relationship between the surface defect and the potential drops, an approximate formula relating measured potential drop to the surface flaw was obtained The present work was initiated to investigate the feasibility of using the technique to detect subsurface cracks and corrosion damage in aircraft skins and panels.

1.2 Theoretical background

The approximate formula mentioned in the Introduction is reproduced in this section for completeness of the exposition. For the purpose of this work, we consider only the two dimensional version of the reconstruction method even though the approach has been extended to three dimensional problems. Suppose we wish to determine the lower curve, $y=\theta(x)$ of the two dimensional domain shown in Figure 1.1. We are given voltage potential reading $V(x)$ on the upper surface, $y=a$. By using potential theory, one can derive a simple relationship between $V(x)$ and $\theta(x)$.

The formula is based on several assumptions: (1) the plate is relatively thin, (2) the defect height is small relative to plate thickness, and (3) the voltage potential in the domain is created by injecting current and removing current at two points on the upper surface.

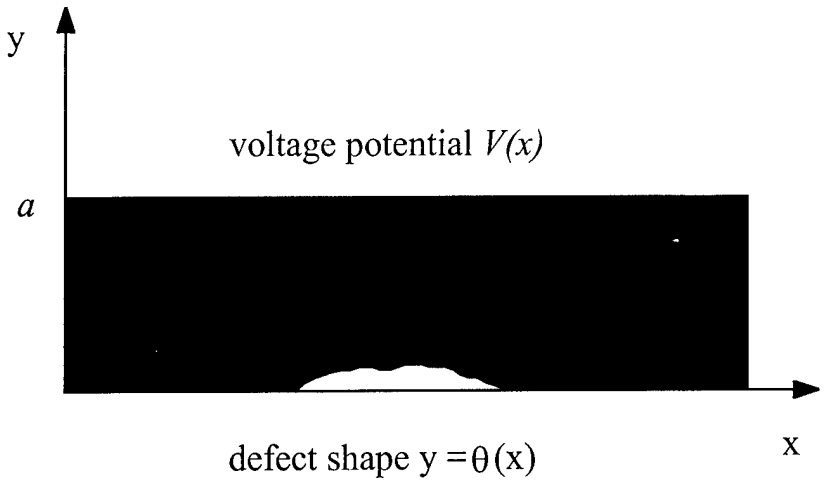

Figure 1.1. A model for the defect determination problem

In order to determine the defect shape $\Theta(x)$, we must know what the voltage response is when the specimen is undamaged. Let us represent the voltage corresponding to the undamaged specimen by $V_o(x)$. If we have continuous reading on the upper surface, the desired formula is:

$$\theta(x) = \frac{\sigma a^2}{I} \frac{d}{dx}[V(x)-V_o(x)].$$

Here, σ is the conductivity of the specimen, and I is the input current per unit length. Having only potential drop readings at distances of Δ allows us to approximate the derivatives on the right-hand side of the above equation. Readers interested in the detailed derivation of the above are referred to [3] and [4].

1.3 Experimental

Although, in principle, the method is capable of reducing data from a two dimensional array, the initial apparatus consisted of a simple linear array of 20 probes attached along the length of the sample. Samples investigated were aluminum, titanium or stainless steel strips typically 1mm x 10mm x 400mm in length into which a variety of defects, such as slots and notches, were introduced. A steady direct current, typically of the order of 4 Amps at 20 Volts, was applied briefly to the probes at the extreme ends of the sample and the voltage drop between each pair of probes was measured, producing 19 data points. This was achieved by attaching the probes to a multiplexer which was in turn connected to a computer running a short LabVIEW™ program: the program measured each pair of probes sequentially and stored the resulting data file. The entire data collection process takes less than 2 seconds.

The signals detected were of the order of microvolts and it was found to be necessary to reduce as far as possible all sources of error such as those which might arise, for example, due to variations in contact resistance and heating at the contact points. Consequently, a macroscopically defect-free but otherwise identical test specimen was used in each case to generate a baseline or background signal which was subsequently subtracted from the actual test signal. In addition to removing sources of systematic error these samples also increased the effective sensitivity of the method.

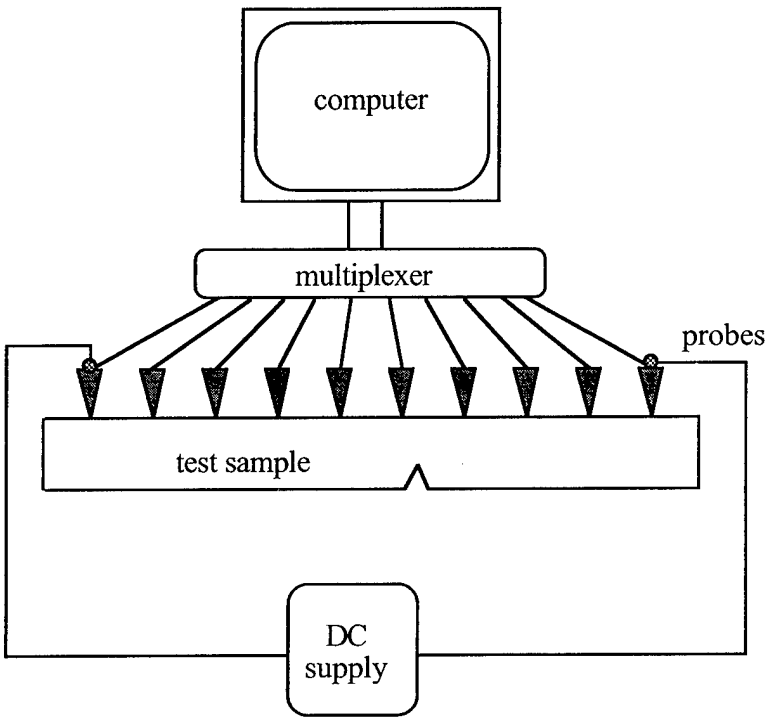

Figure 1.2. Schematic of experimental apparatus

1.4 Results

It was found that the major portion of the applied potential drop occurred between the outer pairs of probes where the current was applied and that the potential drops between probe pairs 3-17 were the most useful. Figure 3 presents raw data without subtraction of the background and shows the results of tests performed on stainless steel samples containing (a) one central slot and (b) two off-center notches. It is seen that the defects are clearly detected and also that they are located at the correct position on the sample.

Examination of the Fig. 3 shows, however, that there is an overall curvature to the data which is particularly noticeable at the ends of the sample, corresponding approximately to data points 3-6 and 16-18. Subtraction of the background greatly reduced this curvature at the ends of the test piece and improved the overall visibility of the peaks as shown in Figs. 4(a)&(b): the peak stands out clearly against a background which is now generally flat. Indeed, the background subtraction was needed for determining the defect profile as pointed out in the previous section.

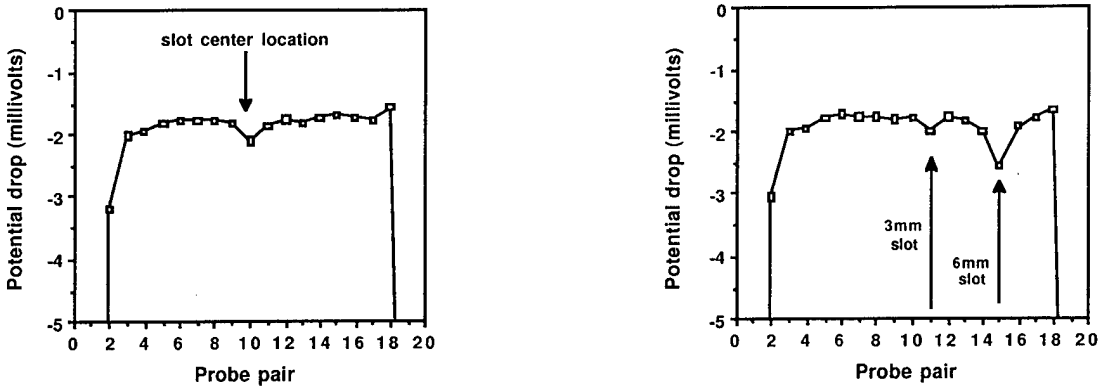

Figure 1.3: Data from samples containing (a) one slot and (b) two notches.

From the specifications of our experimental set-up and using the formula relating voltage potential difference and the defect profile, we estimated the depth of the notch in the single defect case to be 2.6mm, whereas the actual depth was 4mm. We believe the discrepancies are attributable to the measurement errors as well as to the uncertainties in the conductivity of the specimen, as well as some unaccounted for phenomena, such as contact impedance. Nevertheless, we find the results to be encouraging.

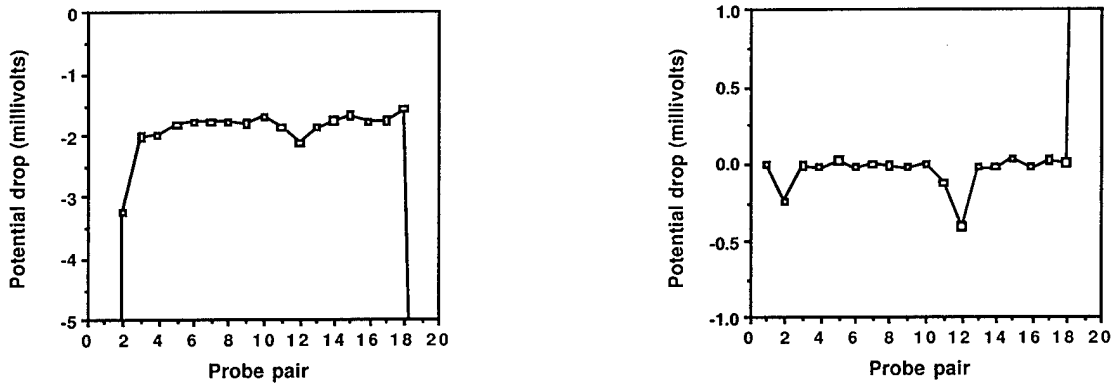

Figure 1.4: Data (a) before and (b) after modification by subtraction of background

1.5 Discussion

The results presented above clearly show that a nondestructive evaluation procedure based on electric potential measurements is capable of locating and quantifying defects and has potential for application in the field of non-destructive evaluation of engineering materials. Although this work has only examined one dimensional arrays of probes, other theoretical work [4] has shown that the method can be applied analogously to 2-dimensional arrays to allow the detection and quantification of defects on rear-surfaces.

At this stage, the limitations to further practical application of the method have become apparent and are principally related to the problems of signal generation, detection and amplification. The potential drops recorded between probes are a function of many factors including, most importantly, resistivity of the test-piece, dimensions of test piece and the applied current. In the examples illustrated here, with a probe separation of 10mm and samples with a cross sectional area of ~10mm^2 and resistivity of ~800$\mu\Omega$.mm, potential differences were of the order of 100 microvolts. The apparatus was easily able to detect defects which occupied 10% of the local cross-sectional area of the sample and, theoretically, this detection efficiency can be substantially improved since the detected signal is mathematically simply related to the dimensions of the actual defect present. However, further substantial improvement in the detection and quantification of defects will depend upon considerably more sensitive and reproducible data collection apparatus.

Also, in order to reduce the detection limit in absolute terms, the probe array spacing would have to be reduced. The problem then becomes one of generating a sufficiently large potential drop across a sample of reduced resistance, necessitating a greatly increased impressed current. Increasing the current could lead to undesirable heating effects which would disturb the potential distribution within the sample. Thus, although it has been demonstrated that the method is capable of yielding the type of results predicted by the previous theoretical work, it has been found that application of the method to practical situations for metallic structures currently presents considerable difficulties. The major difficulty resides in generating a sufficiently large signal for accurate measurement and it is likely that further progress in this application area will have to await more sensitive and rapid voltage measurement devices.

1.6 Conclusions

An electrostatic nondestructive evaluation method has been shown to be a potentially useful method to enable flaw detection in hidden surfaces. A variety of defects have been detected, sized and accurately located. However, further development of the system for metallic (low resistivity) materials will require significant efforts in the amplification and handling of signals in the microvolt range.

1.7 References

[1] F. Santosa and I. W. Hall. Final Report, 1996.
[2] "Nondestructive Inspection of Aging Aircraft", Valley, Del Grande, and Kobayashi, eds., Proceedings of SPIE, volume 2001, 1993.
[3] P. Kaup and F. Santosa, Nondestructive evaluation of corrosion damage using electrostatic measurements, Journal of Nondestructive Evaluation, 14 (1995), 127-136.
[4] P. Kaup, F. Santosa, and M. Vogelius, A method for imaging corrosion damage in thin plates from electrostatic data, to appear in Inverse Problems.

Section 2
"Corrosion of Metal Matrix Composites"

2.1 Introduction

Metal matrix composites (MMC's), particularly those based upon aluminum alloys, are now relatively well-known and are expected to be used in the aerospace industry in a variety of applications. Although they have been under development for many years, the major emphases until recently have been on manufacturing routes and the development of adequate mechanical properties. As these materials mature and are poised to enter service, other properties, including corrosion resistance, are coming under closer scrutiny since there is no reason *a priori* to expect that MMC's will resemble the corresponding unreinforced matrix alloys.

Many of the alloys used in MMC's are the same as are found in current aircraft. This portion of the study was proposed under the aegis of the Aging Aircraft Initiative, therefore, to provide more information about the corrosion of a family of materials, some of which are found in current aging aircraft and some of which will certainly be found in future generations of aircraft. In the latter respect, the research may be considered as attempting to *pre-empt* potential future problems associated with aging of aircraft.

Previous studies of corrosion in aluminum MMC's have been comprehensively reviewed quite recently by Lucas and Clarke [1] and by Hihara and Latanision [2]. However, much of the current literature focuses principally on aluminum alloys reinforced with SiC whiskers or particles whereas alumina particulate MMC's have received considerably less attention. The present work, therefore, addressed both Al/Al_2O_3 particulate MMC's as well as SiC MMC's.

Considering firstly Al/Al_2O_3 composites, Hihara and Latanision reported results from work mainly on FP™ alumina fibers and concluded that there was little effect of the presence of the fibers since no galvanic coupling occurs. Yang and Metzger [3] studied an Al-2Mg alloy containing the same fibers and concluded that the pits observed after immersion in NaCl solutions containing H_2O_2 were attributable to preferential attack of Mg_2Al_3 particles: no preferential attack was observed at the fiber/matrix interfaces. Roper and Attwood [4] studied Al_2O_3/2124 (and SiC) particulate reinforced composites and found no real evidence for a deterioration of the corrosion behavior due to the presence of alumina (or SiC) particles. Differences in the pitting potentials (E_{pit}) were small and were ascribed to experimental scatter. Nevertheless, they pointed out that the solution used for testing, de-aerated 0.1M lithium perchlorate, was not aggressive.

Nunes and Ramanathan [5] also compared a series of Al-7.5%Si-1%Mg MMC's, reinforced with either Al_2O_3 or SiC particles, and concluded that weight loss was more

severe and pitting deeper in the SiC_p MMC's than the Al_2O_3 MMC's. They also found that E_{pit} values were not significantly affected by aeration of the solution. Shimizu *et al.* [6], using de-aerated 3.5%NaCl, found that the presence of alumina or carbon fibers, and silicon carbide whiskers did not affect the pitting potential of Al 6061 and that pit initiation sites were not restricted to any specific sites such as the reinforcement matrix interface but were distributed randomly throughout the surface of the samples.

There is to date, then, little clear evidence that the presence of Al_2O_3 particles seriously adversely affects the corrosion resistance of aluminum alloys, however, it must be pointed out that most of the data has been collected from short term tests or from tests in de-aerated conditions. Also, potentiodynamic scan tests are not always indicative of long-term behavior since the effects on the initiation of pitting must be distinguished from the effects on the propagation of pits. Pit initiation is mainly determined by the location and number of sites whereas the growth rate is kinetically controlled and will be better reflected in long-term immersion tests rather than short-term polarization tests.

The principal objective of the present study was, therefore, to investigate further the early stages of pitting in a specific composite and to cast further light on the effect of the particles *per se* on the corrosion behavior. Experiments were designed so as to separate, as far as possible, the effects of the presence of the particles themselves from the effects which they exert on the matrix microstructure due, for example, to the generation of residual stresses or modification of precipitation sequences.

SiC reinforcements, on the other hand, have received rather more attention in the literature, nevertheless the large variety of base alloys and reinforcement types can make the comparison of results somewhat difficult at first. Trzaskoma *et al.*, studied the corrosion behavior of SiC_w-reinforced Al alloys in 0.1M NaCl solution [7]. They could not detect any difference in the propensity for pit initiation between the MMCs (SiC_w/Al 6061 and SiC_w/Al 5456) and their base alloys. However, they reported that the SiC_w/Al 2024 MMC exhibited a greater susceptibility for pit initiation than the wrought alloy, and attributed it to the increased copper precipitation in the matrix in the presence of the SiC whiskers. The effect of microstructure on the corrosion process, especially the role of secondary phases, has also been reported in the literature [8,9].

Sun, *et al.* and Buarzaiga *et al.* investigated the corrosion behavior of powder metallurgy processed SiC_p/Al MMCs and as-cast SiC_p/Al MMC's respectively [10,11]. They both reported that the extent of pitting increased as the volume fraction of SiC_p increased in the alloys. Buarzaiga *et al.* reported that pit initiation sites varied with Cl^- ion concentration in the electrolyte. Conflicting results have been reported in literature regarding pit initiation sites. Trzaskoma [12] reported that pitting did not occur at interfacial sites while Aylor and Moran [13], and Maahn and Roepstorff [14] reported that the matrix-reinforcement interface was the preferred site for pit initiation.

The present study addresses the following issues:

(i) The extent and nature of the corrosion attack on Al_2O_3/Al MMCs
(ii) The extent and nature of the corrosion attack on SiC_p/Al MMCs
(iii) The effect of SiC_p volume fraction on the corrosion/pitting resistance of the MMC
(iv) The effect of microstructure on pit initiation and propagation
(iv) The effect of fabrication method on the corrosion resistance of the MMC and
(v) Comparison of the corrosion behavior of the unreinforced alloy and the reinforced alloy to delineate the influence of the various particulate reinforcements.

2.2 Experimental

2.2.a Material

The specific Al_2O_3-reinforced composites used in this study are intended for use in conventional casting operations and had been fabricated by a liquid metal route in which the particles were dispersed in the molten alloy and held in a cupola for some time before casting and subsequent processing by conventional metalworking procedures. The 6061-Al composite, containing 15 vol.% (V_f%) Al_2O_3 particulate reinforcement, and the corresponding unreinforced alloy were obtained as rolled planks, 19x78mm in cross-section, in the naturally aged T4 condition (2 hrs. at 530°C, water quench). Some samples were also subsequently heat treated to the T6 condition by solution treatment for 2 hrs. at 560°C, water quenching and aging for 10 hrs. at 177°C. The composition of the composite is given below as Table 1.

Table 1. Composition of composite

Al	Si	Fe	Cu	Mn	Mg	Cr	Ti	Zn	Al_2O_3
bal.	0.63	0.2	0.27	0.01	1.00	0.10	0.12	0.07	14.9 v/o

The SiC_p materials for the study were supplied by Lanxide Corporation, Newark, DE, and manufactured by their PRIMEX™ pressureless metal infiltration process. Five categories of materials were supplied in the as-cast condition, namely: unreinforced Al-10%Si-1%Mg alloy, and the same alloy reinforced with 20V_f%, 30V_f%, 40V_f% and 55V_f% SiC particulates, respectively. The samples were all given a simulated T4 heat treatment by annealing at 500°C for two hours to homogenize and ensure comparable initial matrix microstructures.

Samples approximately 1cm^3, were sectioned from the bulk material using a diamond saw. After heat treatment, the samples were polished to 120 grit to remove any scale. A copper wire was attached to ensure good electrical contact and the sample was then mounted in epoxide resin. Finally, the top surface of the samples/working electrodes were polished to 0.25μm diamond.

2.2.b Immersion testing

Long-term weight loss and conventional immersion tests were carried out on T4 heat treated Al_2O_3/6061 MMC specimens immersed in 3.5 wt% NaCl solution of pH 8.2 at 22±0.5°C for periods up to 123 days. Based on ASTM recommendations [15] and availability of material, the weight loss specimens were 100x15x2.5mm in size. Immersion specimen dimensions were 10x10x10mm. Specimen surfaces were polished to 600 grit finish before testing. Before each weight loss measurement, and also for metallographic examination, specimens were gently washed with 0.5% H_3PO_4 to remove corrosion products then cleaned with de-ionized water and alcohol.

2.2.c Electrochemical corrosion testing

Cyclic polarization (CP) and/or potentiodynamic scan (PD) testing was conducted on both T4 and T6 heat treated specimens. A Princeton Applied Research Model 273 potentiostat/galvanostat, driven by an EG&G Princeton Applied Research Model 352/252 SoftCorr II software package was used to record all the tests. A graphite electrode was used as the counter electrode, and a Ag/AgCl electrode saturated with 4M KCl solution was used as the reference electrode. The scans were generally performed from 500mV negative to the corrosion potential until the critical pitting potential and then reversed to the protection potential. A variety of scan rates were investigated and all tests were conducted at 23±1°C. Although the principal interest of course centers upon corrosion in simulated service conditions, both aerated and de-aerated environments were used. For the de-aerated environment testing, 99.99% argon was bubbled through the solution for two hours before testing and continued throughout the experiment.

Cyclic polarization tests yield a variety of information concerning the corrosion behavior of the specimen. As the potential of the sample is increased the current decreases at first until the corrosion potential, E_{CORR}, is reached, at which point it drops to (effectively) zero as this is the potential at which forward and reverse reactions are identical so no net current flows. When the sample is further polarized the current increases until a region may be encountered during which activation and concentration polarization prevent further increase of current density. In this condition, corrosion is generally proceeding through a continuous and somewhat protective oxide film. At sufficiently high potentials, the film is broken down locally and rapid attack occurs forming pits, this is the pitting potential, E_{PIT}. As the potential is further increased, pitting becomes more and more severe.

When the scan is reversed and the potential reduced, the tendency to pitting decreases and a potential is reached at which pitting ceases, the sample repassivates, E_{REP}, and the protective oxide layer can re-form. This potential is, therefore, a measure of the ease with which the protective layer can reform after pitting. Further reducing the potential causes a corresponding reduction in the corrosion current density, another vertical linear segment may be encountered, but then a new value of the corrosion potential will be measured, E_{fCORR}. The difference between initial and

final values of the corrosion potential is a measure of the severity and irreversibility of attack. These parameters are illustrated schematically in Fig. 1.

2.2.d Microscopy

Microstructural analysis of metallographically polished samples was performed before and after corrosion by optical microscopy and scanning electron microscopy (SEM) using a JEOL JXA 840. A limited amount of transmission electron microscopy (TEM) was performed on a Philips EM400T after sample preparation by standard ion milling procedures. Energy dispersive X-ray spectroscopy (EDS) was used in both the SEM and TEM.

2.3. Results

For clarity, the complete results for the Al_2O_3/Al and SiC/Al materials will be presented separately, beginning with the former.

2.3.a Al_2O_3/Al MMC

2.3.a.i Weight Loss

Cumulative weight loss for the T4 composite was found to be considerably greater than for the corresponding unreinforced alloy, Fig. 2. The data points are averages from three separate tests and the error bars show the data are highly reproducible. While the unreinforced alloy clearly follows a parabolic rate law (or more probably logarithmic at longer times), it would appear that the weight loss of the composite is parabolic but with a much higher rate constant.

It will be seen below that in both cases the weight loss was highly localized, hence, weight loss *rates* are of little practical value. Nevertheless, with this caveat and purely for comparison purposes, these weight losses correspond approximately to a uniform corrosion rate of 1.5×10^{-2} mm/yr for the composite and 4×10^{-3}mm/yr for the alloy.

2.3.a.ii Electrochemical testing

This type of test gives an indication of whether a material is likely to pit and also distinctly identifies the value of the pitting and protection potentials. The pitting potential is identified during the forward scan and the potential at which the pits repassivate, E_{REP}, the protection potential, during the reverse scan.

Tests were performed at three different scan rates and the scan rate was found to be an important testing variable. It was frequently, but by no means invariably, observed that the slower the scan rate the smaller was the hysteresis area enclosed by the forward and reverse scans. Also, as the scan rate was reduced the initial corrosion potential, E_{CORR}, increased whereas the final corrosion potential decreased: this meant that ΔE_{CORR} (E_{CORR} - E_{fCORR}) decreased. In addition the corrosion currents were also generally reduced. Some of these effects are shown in Fig. 3 for the composite in the T4 condition in de-aerated solution.

All data discussed specifically hereafter were generated at $1mVs^{-1}$ since it is believed that these data may be applicable to actual service conditions while avoiding other complications which will be detailed below. Nevertheless, for completeness, and to provide the possibility of comparison with the results of other workers using different scan rates, all the test data are presented below in Table 2 for all three scan rates.

Table 2. Complete corrosion data for all Al_2O_3/Al samples.
(i) De-aerated solution

Material	Heat Treatment	Scan Rate (mVs^{-1})	E_{CORR} (mV)	E_{PIT} (mV)	E_{REP} (mV)	E_{fCORR} (mV)
Composite	T4	0.1	-1165±24	-669±5	-678±7	-951±2
		1	-1203±14	-669±8	-669±18	-944±10
		5	-1234±14	-656±10	-717±6	-839±7
	T6	0.1	-908.1±15	-684±3	-684±5	
		1	-876±73	-684±4	-707±2	-900±2
		5	-1085±46	-666±14	-724±7	-870±3
Alloy	T4	0.1	-1054±35	-656±2	-666±11	-989±3
		1	-997±24	-661±1	-694±3	-901±1
		5	-926±58	-660±2	-726±7	-821±3
	T6	0.1	-1061	-683	-667	-1037
		1	-1101±59	-671±6	-704±2	-951±3
		5	-1110±106	-662±9	-729±4	-843±3

where E_{CORR} is the initial corrosion potential
E_{PIT} the critical potential for pit nucleation
E_{REP} the repassivation potential
E_{fCORR} the final corrosion potential E_{fCORR}

Table 2 (continued)
(ii) Aerated solution

Material	Heat Treatment	Scan Rate (mVs^{-1})	E_{CORR} (mV)	E_{PIT} (mV)	E_{REP} (mV)	E_{fCORR} (mV)
Composite	T4	0.1	-1145±50	-661±7	-676±4	-940±2
		1	-1221±5	-663±9	-672±6	-914±13
		5	-1235±12	-644±13	-715±9	-816±8
	T6	0.1	-783±83	-682±4	-679±1	
		1	-949±87	-675±4	-661±3	-945±2
		5	-1171±23	-670±2	-736±4	-855±2
Alloy	T4	0.1	-657±50	-651±3	-665±3	-980±5
		1	-952±30	-664±6	-700±10	-868±3
		5	-1028±50	-666±1	-705±5	-790±2
	T6	0.1	-673±5	-660±2	-667±2	
		1	-983±50	-668±4	-720±4	-870±7
		5	-1030±58	-673±6	-717±3	-815±3

The single most consistent parameter among all the tests was the pitting potential, E_{PIT}, which remained essentially constant at ~670±10mV for both reinforced and unreinforced alloy in both heat treated conditions and with or without dissolved oxygen. Similarly, the repassivation potential, E_{REP}, did not show great variability but was shifted ~20mV negative for the composites and >30mV negative for the unreinforced alloy, the largest shift being noted for the unreinforced T6 alloy where the shift was ~50mV negative.

Typical CP scans for the composite and alloy in the T4 condition are shown in Figs. 4(a)&(b). T4 heat treated composite had a significantly lower E_{CORR} than the unreinforced alloy in either aerated or de-aerated solution but, after repassivation, the values of E_{fCORR} were close to those of the unreinforced alloy.

A further effect noted from Fig. 4(b) is that corrosion current oscillations were observed for specific samples and scan speeds. This Figure shows that, during the forward scan, the unreinforced Al6061-T4 sample exhibited large fluctuations in current around E_{CORR}. Figs. 5(a)&(b) show an enlarged view of the same phenomenon in T6 heat treated Al_2O_3/Al6061. This phenomenon was noted in several different samples and, although care was taken to ensure good electrical contacts throughout the

system, it could not be avoided. The oscillations can be interpreted as showing that the sample was switching between two states, one where corrosion was considerably more rapid than the other. This type of behavior was most pronounced at slow scan rates.

Considerable difference was noted between T4 and T6 heat treated samples and typical CP scans for T6 treated samples are shown in Fig. 6(a)&(b) for composite and alloy respectively in both aerated and de-aerated conditions. These Figures should be compared with Figs. 4(a)&(b). Although the pitting and repassivation potentials were not drastically altered, the values of E_{CORR} increased by approximately 300mV for the T6 composite samples in either aerated or de-aerated solution. Similarly for the unreinforced alloy, the value of E_{CORR} increased by approximately 120mV with artificial aging.

2.3.a.iii Metallography

Examination of the unreinforced alloy samples after immersion testing showed that two types of attack occurred, namely, along grain boundaries and also through localized pitting. Immersion and weight-loss samples showed highly localized areas of attack which developed early and where subsequent corrosion was largely concentrated. In contrast, the composite sample exhibited constant pit initiation, in other words it was an ongoing process and the pits did not appear to exert a significant cathodic protective effect on the surrounding material. Fig 7. shows the typical appearance of the composite before immersion while Figs. 8(a) and (b) show the typical appearance of the unreinforced alloy and composite sample respectively after 8 days immersion.

Corrosive attack became steadily worse in the composite and comparisons of the extent of pitting at 8 days and 16 days are presented in Figs. 9(a)&(b). It is clear that, while pitting occurred quite generally throughout the sample, there were nevertheless certain sites at which it was particularly severe. These pits developed into sites which could be up to several 100μm's in diameter. This is particularly clearly illustrated in Fig. 9(c) showing a sample before removal of the layer of corrosion products.

Fig. 10 shows such a pit located at a grain boundary triple point and exhibits extremely deep penetration at the right but only relatively shallow penetration at the left: the location of this major pit at a grain boundary intersection is readily apparent. Also it should be noted that attack is by no means uniform around each particle: some show almost no attack while others have been totally exposed.

The interiors of these deep pits showed cusp-shaped depressions where particles had been, or were being, removed, Fig. 11. The gentle cusp shape of the pits, as opposed to a crystallographically dominated angular pit, is evidence that the pits propagated rapidly since pits with facets developed along specific crystallographic planes are only observed at very slow corrosion rates.

The observation that pitting occurred preferentially at certain locations in the composite, as seen in Fig. 9(b), prompted closer examination and it was found by

examining samples at shorter times that the locations where pitting first occurred fell into two categories. The first was simply associated with agglomerations of particles, particularly when the agglomerations were at grain boundaries.

The second, however, was the more common, more severe, and was associated with a specific site which showed early and rapid pit nucleation while nearby particles were totally unaffected, Fig. 12. These particles were investigated by EDS analysis and it was found that the particles and pit interiors appeared to exhibit a Ti content which was unusually high given the initial Ti content of 0.12%. Subsequently, X-ray mapping of polished but uncorroded samples revealed the presence of a large number of Ti/Zr rich particles which were the same size and shape as the Al_2O_3 particulates and which had previously gone unnoticed. These particles were extremely active pit initiators and the remnants of these particles could be identified in the bottom of almost all the major pits after short immersion times. After longer immersion times, the particles had dissolved completely but the Ti from them remained detectable in the general region of the pit indicating dissolution and re-precipitation as part of an adherent corrosion product.

TEM was then used to investigate the types of precipitate present in the materials. In addition to the common Mg_2Si precipitates, Fig. 13, and a variety of Al-Fe-Mn bearing intermetallics, attention was focused upon the large, ~20μm in diameter, Ti-rich particles discussed above. These were found to be typically polycrystalline and to contain very high concentrations of Ti and Zr in addition to appreciable amounts of Si and Al. Figs. 14(a)&(b) show a typical particle at low and higher magnifications respectively. These show the particles to be composed of a small grain size core while the external surface of the particle has undergone reaction with the molten aluminum to form relatively larger, blocky grains of a titanium/zirconium aluminide phase. Fig. 14(c) shows the EDS spectrum associated with the blocky grains visible at the edge of the particle in Fig. 14(b). The occurrence and effects of these particles are considered further in the discussion section below.

2.3.b Results: SiC_p/Al MMC

2.3.b.i Electrochemical testing

Again, electrochemical testing was performed by means of cyclic polarization tests. This time 4 different scan rates were investigated and the complete data are presented below as Table 3 and each value is the average of at least four tests. Testing under de-aerated conditions generally leads to nobler potentials for the OCP, but the values of the pitting and protection potentials are about the same as those for the aerated tests.

Table 3. Complete corrosion data for all SiC_p/Al samples: (i) De-aerated solution

V_f% SiC	Scan Rate (mVs^{-1})	E_{CORR} (mV)	E_{PIT} (mV)	E_{REP} (mV)	E_{fCORR} (mV)
0	5	-1396±3	-460±5		-848±24
	1	-1323±3	-652±8		-959±31
	0.167	-1197±24	-726±10	-722.7	-985±39
	0.1	-1169±10	-722±7	-722.7	-1032±20
20	5	-1264±30	-675±5	-720±3	-942±10
	1	-1120±30	-690±3	-703±2	-900±15
	0.167	-1075±15	-692±5	-716±2	-890±10
	0.1	-871±10	-705±4	-717±2	-897±10
30	5	-1237±18	-690±8	-731±7	-940±16
	1	-1201±25	-700±4	-723±3	-958±4
	0.167	-1144±6	-707±8	-719±1	-940±6
	0.1	-1028±20	-704±12	-722±12	-928±8
40	5	-1105±20	-325±10	-737±10	-880±20
	1	-1200±26	-645±5	-739±10	-835±45
	0.167	-962±94	-702±2	-700±2	-875±33
	0.1	-870±3	-709±5	-713±2	-804±35
55	5	-1339±5	-658±7		-924±11
	1	-1303±5	-678±10	-720	-870±15
	0.167	-1225±10	-697±10	-692	-876±10
	0.1	-1000±10	-710±10		-1008

Table 3 (continued)
(i) Aerated solution

V_f% SiC	Scan Rate (mVs^{-1})	E_{CORR} (mV)	E_{PIT} (mV)	E_{REP} (mV)	E_{fCORR} (mV)
0	5	-1290±18	-465±2		-828±10
	1	-1174±19	-671±3		-811±16
	0.167		-711±10	-719	-1013±6
	0.1		-719±10	-706	-1010±5
20	5	-989±29	-688±6	-743	-836±4
	1	-958±43	-697±4	-721	-890±5
	0.167	-964±20	-707±10	-759	-826±10
	0.1		-700±10	-703±5	-889±10
30	5	-1254±26	-709±3	-749	-901±6
	1	-1223±9	-706±4	-737	-936±8
	0.167		-714±3	-713	-926±5
	0.1		-697±5	-705	-894±5
40	5	-1118±25			-889±21
	1	-913±29	-655±7		-726±7
	0.167		-765±39		-782±32
	0.1		-720±4		-715±2
55	5	-1370±16	-644±30	-719±3	-890±27
	1	-1243±45	-688±6	-718±9	-975±36
	0.167				
	0.1		-709±2		

For ease of presentation, the principal parameters are also tabulated as Table 4 and presented graphically as Figures 15(a)&(b).

Table 4: Principal parameters at scan rate of 1mV/sec

	De-aerated			Aerated		
V_f% SiC	E_{CORR} (mV)	E_{PIT} (mV)	E_{fCORR} (mV)	E_{CORR} (mV)	E_{PIT} (mV)	E_{fCORR} (mV)
0	-1323±3	-652±8	-959±31	-1174±19	-671±3	-811±16
20	-1120±30	-690±3	-900±15	-958±43	-697±4	-890±5
30	-1201±25	-700±4	-958±4	-1223±9	-706±4	-936±8
40	-1200±26	-645±5	-835±45	-913±29	-655±7	-726±7
55	-1303±5	-678±10	-870±15	-1243±45	-688±6	-975±36

From the above and Figs. 15(a)&(b), it is quite clear that, at constant scanning rate of $1mVs^{-1}$, there is no significant variation in pitting potential in either aerated or de-aerated solution as the $V_f\%$ SiC_p increases. In addition, for each different $V_f\%SiC$, the values of E_{PIT} are essentially identical in both aerated and de-aerated solution. The value of E_{fCORR} was generally at considerably more active potentials than E_{PIT}, the actual values being about 200mV negative for de-aerated solution. It is noticeable that while the values for 20,30 and $40V_f\%SiC$ samples were relatively unchanged by aeration, the values for 0% and $55V_f\%SiC$ were markedly changed, the former by ~150mV noble and the latter by ~100mV active.

Again it was found that the scanning rate had a fairly consistent effect on the nature of the curves, in particular, the values of E_{CORR} decreased while those of E_{PIT}, tended to increase with increasing scanning rate.

Typical cyclic polarization curves for the unreinforced alloy are presented in Fig. 16 which shows that both E_{CORR} and E_{fCORR} are lower in deaerated solution, while the values of E_{PIT} are substantially similar. It is also observed in this and many other cases that an additional 'knee' occurs on the polarization curve. This knee occurred generally in the range -650 to -700mV and was unaffected by the $V_f\%SiC$ and must, therefore, be attributed to a matrix effect rather than due to the reinforcement. At this point it is believed to be associated with the porosity which is present in the samples and will be illustrated below.

Fig. 17 shows a series of scans for different $V_f\%SiC$ samples tested in aerated solution and the absence of consistent correlation with volume fraction of reinforcement particles is readily appreciated.

Again it was found that cyclic polarization testing at the slowest scan speeds tended to produce 'noisy' scans similar to that previously illustrated in Fig. 5 where the sample is in a metastable state.

However, despite multiple testing on many samples of each material, no truly systematic, monotonic variation of corrosion parameters was found as a function of $V_f\%$ reinforcement. It will be seen below that a major reason for this is probably to be found in the composite's microstructure.

It was observed during the tests that there was vigorous gas evolution at the counter electrode (graphite-hydrogen) and the sample surface (oxygen), during the anodic polarization portion of the scan for all specimens.

2.3.b.ii Metallography

The optical microstructure of the unreinforced Al-Si alloy showed a coarse dendritic structure with slightly rounded platelets of acicular silicon eutectic, Fig. 18(a), and intermetallic phases, notably the light gray Al-Si-Mg-Fe phase present in blade-like and plate morphologies, $FeMg_3Si_6Al_8$; other intermetallic particles were also identified

in the SEM by EDS. These intermetallics did not appear to nucleate preferentially on the SiC particles. It was also clear that the samples contained appreciable interdendritic shrinkage porosity, Fig. 18(b) and these were predominantly the areas attacked during the electrochemical and/or immersion tests of unreinforced alloy. Fig. 19 shows the results of a 16 day immersion tests on the unreinforced alloy which has produced mild attack at the pre-existing porosity but also caused attack of a population of intermetallic particles.

The addition of SiC particles caused a change in microstructure from dendritic to fine cellular, with the SiC_p and Si eutectic residing primarily at the cell boundaries, Fig. 20(a). The particles were homogeneously distributed and the porosity was found to be on a much smaller scale and well distributed throughout the structure, Fig. 20(b).

After cathodic polarization testing of the 20%SiC MMC, it was found that attack was concentrated at a few well-separated regions. Fig. 21(a) shows a low magnification view of a sample (which had been previously marked out into segments to enable examination of areas before and after corrosion) in which the typical attack is shown. Higher magnification shows an apparently progressive intergranular, or intercellular, attack in which the matrix is steadily removed, leaving the reinforcing particles and eutectic Si platelets in place, Figs. 21(b)&(c).

The situation was more severe for the 30%SiC MMC, and Figs. 22(a)&(b) show low magnification views of the same area before and after cyclic polarization testing. The extent of the attack is considerably greater than for the 20% composite although the same general trend is observed for severe attack in some areas while other regions are relatively untouched. At higher magnification, Figs. 23 a)&(b), it is seen that there is fine microporosity present before corrosion and that the particles and silicon are left outlined by subsequent corrosion. Similar observations were made for the 40% and 55% SiC MMC's also and Figs. 24(a)&(b) show the effects of electrochemical testing on the 55%SiC composite.

4. Discussion and Conclusions

This section begins by considering first the Al_2O_3/Al-6061 system. The shift in repassivation potential may be considered as a measure of the difficulty of re-forming the protective oxide layer on the surface of the material after pitting, a large shift indicating serious damage while a small shift indicates that a protective film is easily formed. The shifts noted for the Al/Al_2O_3 composites indicate that, while pitting had occurred, it was relatively easy to repair the film in most cases, the greatest difficulty being found for the unreinforced T6 alloy although this was, again, only a small shift.

The reduction in ΔE_{CORR} noted for the composite in the T4 condition indicates that, after one cycle of the polarization test, the composite should behave similarly to the unreinforced alloy. This represents an improvement in corrosion behavior and supports the view that anodization may offer useful benefits under certain

circumstances. Also, it should be noted that heat treatment can have a significant effect on corrosion parameters, the Al_2O_3/Al-6061 MMC being more corrosion resistant in the T6 condition than in the T4 condition as shown by comparison of Fig. 4(a) and Fig. 6(a). Since the heat treatments affect the matrix microstructure and not the disposition of the particles, it is reasonable to conclude that the matrix controls the corrosion potential, while the particles exert control mostly over the pitting potential.

The unavoidable oscillations in corrosion current during the forward scans of some specimens are believed to be due to a dynamic balance between corrosion and film formation The more rapid of the corrosion processes led to production of a protective film which subsequently caused a decrease in corrosion rate to the lower value. In a short while, however, more rapid corrosion again occurred at another site and the cycle was repeated. The implication of these oscillations is that, if the sample were to be left at constant potential it would corrode more freely but that the increasing potential aids in re-passivation and reducing the corrosion rate. The oscillations were principally observed at the lowest scan rates where there was sufficient time for film formation. The effect of scan speed on the test results was also remarkable and should be noted since it may indicate why inconsistencies exist in the literature for this and other MMC systems.

Perhaps the most significant finding though, is contained in the weight loss data which show a significantly greater corrosion rate for the composite when compared with the unreinforced matrix. The fact that these rates differ initially by a factor of approximately three is especially significant since the principal corrosion process is pitting and not uniform general corrosion. This indicates that, at short times, Al_2O_3/Al composites may be anticipated to undergo more rapid corrosion than the corresponding unreinforced alloy but that, at longer times, they may be expected to corrode at similar rates. The difference in the corrosion rates may be related to the presence of the large Ti/Zr particles.

The effect of the large Ti/Zr rich particles is especially worthy of note since they present several complications not noted before in this type of MMC. First, they have been shown to influence the pit initiation process very strongly indeed since they are highly active anodic regions which corrode very rapidly. Although the particles are attacked at once, the pits they produce persist and Ti remains in the vicinity combined in a corrosion product. Similar behavior has been noted in Cu-containing alloys and SiC_w composites [16] in which a Cu-plated layer has been observed to occur on the SiC whiskers.

Second, the presence of the Ti-rich particles is not anticipated from the overall chemical analysis of the composite in which Ti and Zr were measured at their usual low levels. It is believed that these particles arose as a result of the agglomeration of grain refinement additions which are made to this and many other aluminum alloys. Such additions typically contain TiB_2, for example, and it is probable that boron was also present but not detected by the EDS system used. During the subsequent period, in

which the alloy was held molten and the SiC particles were dispersed, the grain refining additions produced the large agglomerations detected here.

In the present case, corrosion of the composite is more serious than that of the unreinforced alloy but it is highly probable that this effect may be easily remedied by a simple modification of casting-shop practice, i.e. making the grain refinement additions immediately before casting the composite, or not at all. Nevertheless, this provides a clear example of where the deterioration in the corrosion properties is not due to the presence of the reinforcement itself but to the modification of the processing route.

Although weight loss experiments were not performed, it was qualitatively clear from the immersion tests that the SiC_p/Al-10Si MMC's were more prone to corrosion than the Al_2O_3/Al-6061 MMC. No clear relationship was observed, however, between V_f%SiC and the electrochemical parameters of corrosion but, nevertheless, it appears that the addition of increasing the V_f% of SiC_p by itself did lead to degradation of corrosion resistance. This can be seen by comparing Figs. 22(b) and Fig 21(a). The reasons for this are presently unclear but several factors are involved.

First, the Al-10Si/SiC_p MMC's contained an appreciable amount of porosity which no doubt complicates the corrosion behavior by providing a) sites which already present *de facto* pits and b) sites which may be repassivated only with greater difficulty. Further studies will be necessary to separate the effects of porosity from the effects of the presence of the particulate reinforcement.

In general, this work has also demonstrated the importance of intermetallic particles in the corrosion process. The large Ti/Zr intermetallics are obvious and extreme examples but similar effects are shown in Fig. 19 where one of the types of intermetallic particles has been removed by corrosion, leaving the Si eutectic unattacked. There is no evidence from the present work to show that the reinforcement particles themselves contribute to increased corrosion through phenomena such as galvanic effects or the introduction of a greater number of interfaces. Effects which are observed are principally due to microstructural changes in the matrix which are brought about by the addition of reinforcing particles. For example, the addition of SiC_p causes a general reduction in the size of the porosity in the Al-10%Si samples, leading to a larger number of potential pit initiation sites and this is what is reflected in the general observations of corrosion in these samples.

A further significant observation which has emerged in this research is the importance of sample preparation in such corrosion work. Most studies to date have tended to use surfaces prepared to ~600 grit finish but this has been found to give results which are not highly reproducible. In addition, the length of time between preparation and testing, the length of time the sample was allowed to achieve stable open circuit potential before testing, and the length of time since heat treatment were all found to be important. Much greater consistency was achieved when the following points were observed.

- Samples should be metallographically polished to ~3μm before testing.
- After metallographic polishing the samples are highly reactive, presumably because of the recent removal of the protective oxide layer. Significant differences in the corrosion parameters were found for samples which were tested within an hour or so of polishing and those which were tested several days or weeks later. This is ascribed to the ongoing process of repair of the oxide film.
- Samples should be allowed to equilibrate in the experimental conditions for at least 2 hours prior to testing.
- Samples which are susceptible to room temperature aging phenomena should be tested at constant aging time.

When these conditions were implemented in the later stages of testing, experimental test data became significantly more consistent.

Acknowledgments

The author gratefully acknowledges Duralcan (USA) Ltd. for provision of the Al_2O_3/6061 Al composite and alloy and Lanxide Corporation. for provision of the SiC_p/Al-Si composite and alloy.

References

[1] K. A. Lucas and H. Clarke, "Corrosion of Aluminium-Based Metal Matrix Composites", Wiley & Sons. Inc., New York, 1993.
[2] L. H. Hihara and R. M. Latanision, Int. Metall. Rev., 39 (1994) 245.
[3] J. Y. Yang and M. Metzger, Electrochem. Soc. Abstract No. 155, **82-2**, (1981).
[4] G. W. Roper and P. A. Attwood, J. Matls. Sci., **30** (1996) 898.
[5] P. C. R. Nunes and L. V. Ramanathan, Corrosion Science, **51** (1995) 610.
[6] Y. Shimizu, T. Nishimura and I. Matsushima, Matls. Sci. Eng. A, **A198** (1995) 113
[7] P. P. Trzaskoma, E. McCafferty and C. R. Crowe, J. Electrochem. Soc., **130** (1983) p. 1804.
[8] K. R. VanHorn., "Aluminum:Properties, Physical Metallurgy and Phase Diagrams", **1** (1967) ASM, OH, p.212.
[9] P. P. Trzaskoma, Corrosion, **46** (1990) p. 402.
[10] H. Sun, E. Y. Koo and H. G. Wheat, Corrosion, **47** (1991) p.741.
[11] M. M. Buarzaiga, and S. J. Thorpe, Corrosion, **50** (1994) p.176.
[12] P. P. Trzaskoma, E. McCafferty and C. R. Crowe, Extended Abstract 152, Electrochem. Soc. Denver Mtg., (1981).
[13] D. M. Aylor and P. J. Moran, J.Electrochem. Soc., **132** (1985) p. 1277.
[14] E. Maahn and S. Roepstorff, 12 Risø Int. Symp. on Mat. Sci., Risø, Denmark (N. Hansen et al, eds.) 1991, p. 497.
[15] "Standard Practice for Laboratory Immersion Corrosion Testing of Metals", ASTM Corrosion Standard G 31-72, ASTM, (Phila. PA.) 1990.

Additional References

Some further details of this work may be found in the following:

1. Corrosion Mechanisms of Aluminum Matrix Composites", L. Bao, M.M.S.E. Thesis, University of Delaware, 1996.
2. Corrosion Behavior of 6061 Aluminum and 6061 Al/Alumina Particulate Reinforced Metal-Matrix Composite", G. Li, M.M.S.E. Thesis, University of Delaware, 1996.

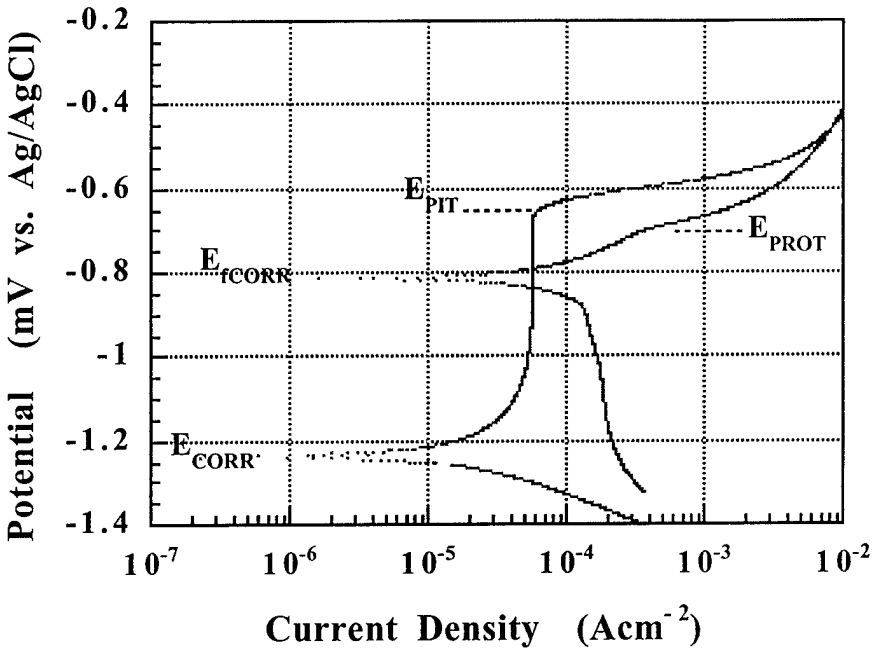

Fig. 1. Schematic cyclic polarization curve showing location and definition of principal parameters measured.

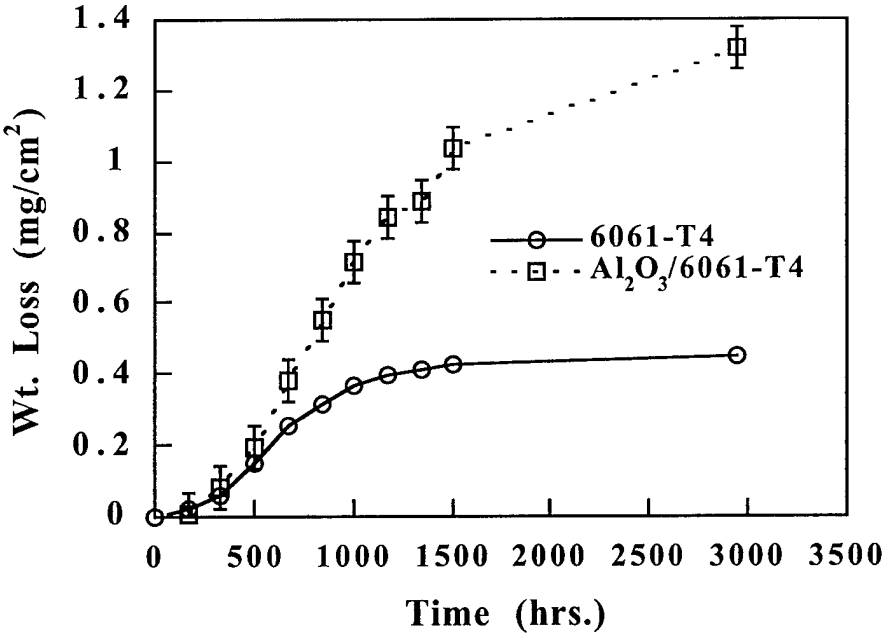

Fig. 2. Wt. loss *vs.* time for the Al_2O_3/6061-T4 composite and unreinforced alloy.

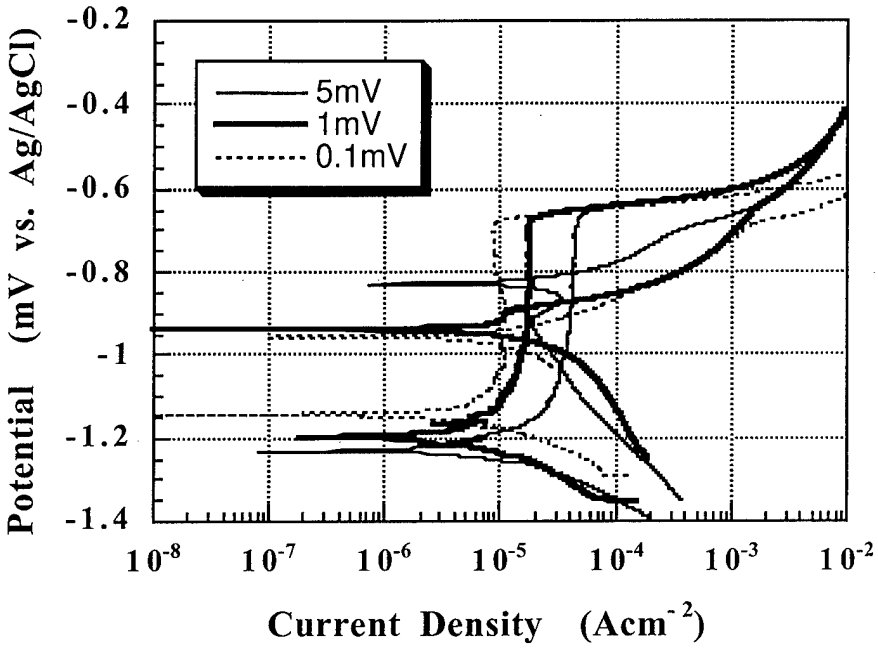

Fig. 3. Effect of scan rate on measured corrosion behavior of Al_2O_3/Al6061-T4 composite.

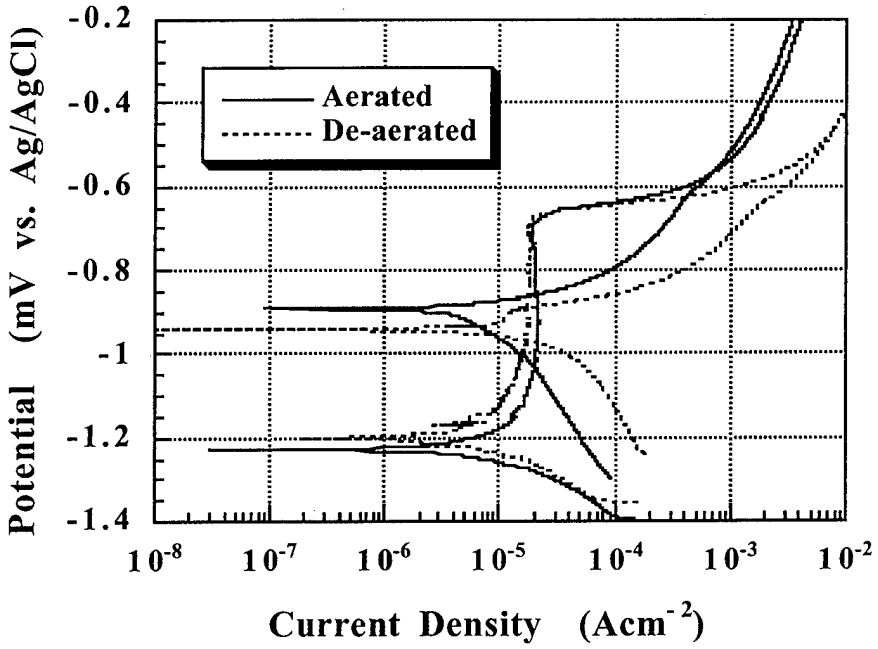

Fig. 4(a) CP scans for Al_2O_3/Al6061-T4 composite.

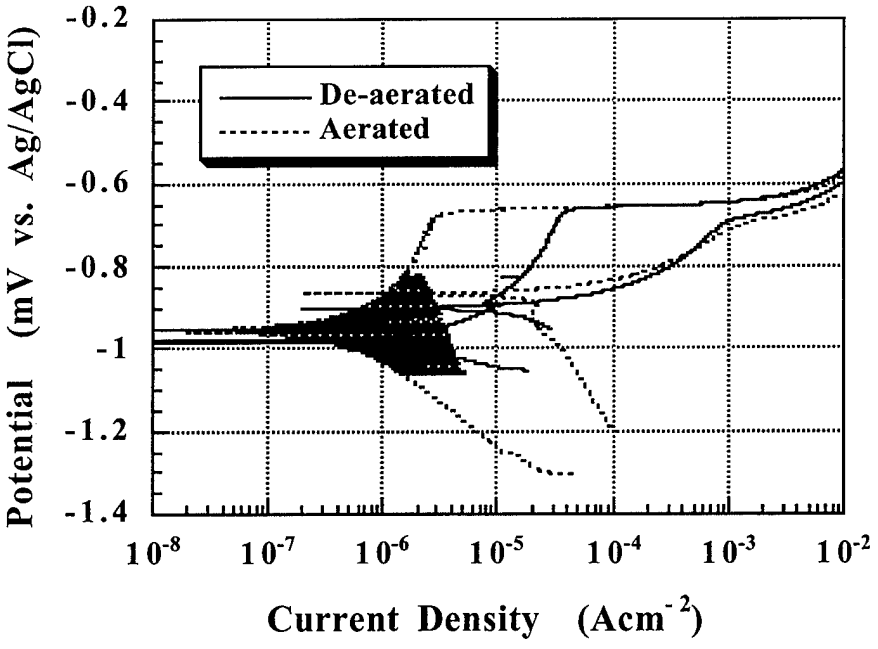

Fig. 4(b) CP scans for unreinforced Al6061-T4.

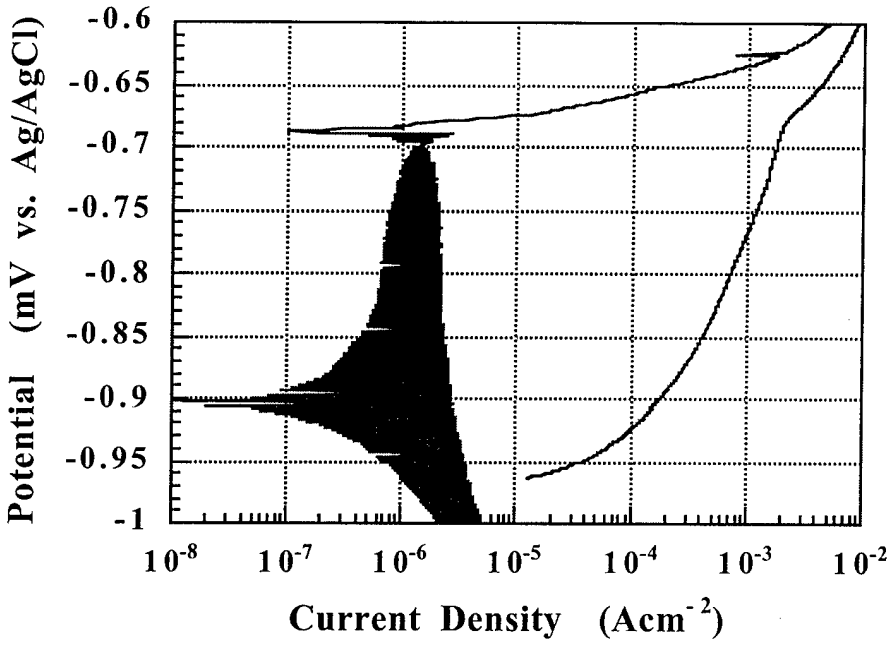

Fig. 5(a) CP scan for Al_2O_3/Al6061-T6 at $0.1mVs^{-1}$ showing corrosion current oscillations around E_{CORR}.

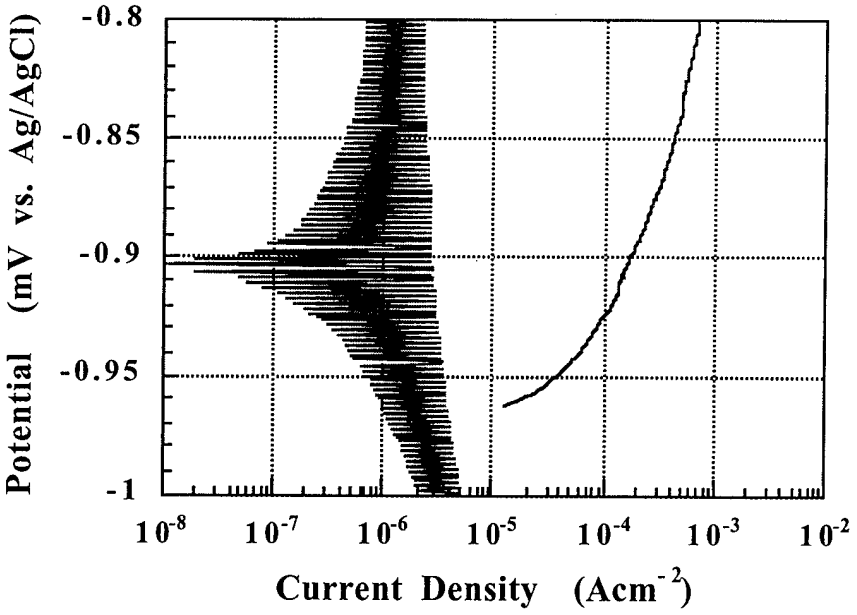

Fig. 5(b) Enlarged section of Fig. N(a) showing corrosion current oscillations.

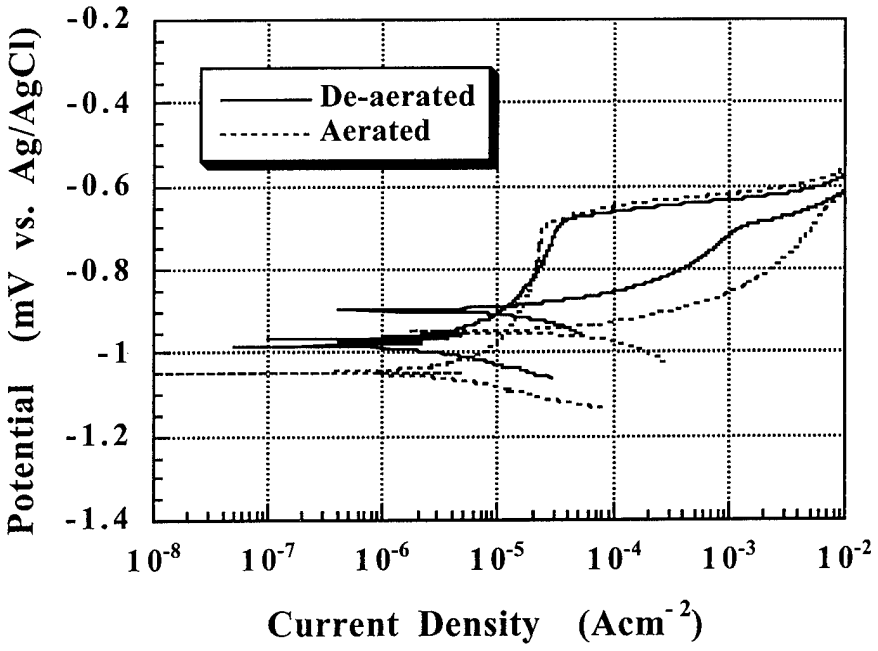

Fig. 6(a) CP scans for Al_2O_3/Al6061-T6 composite.

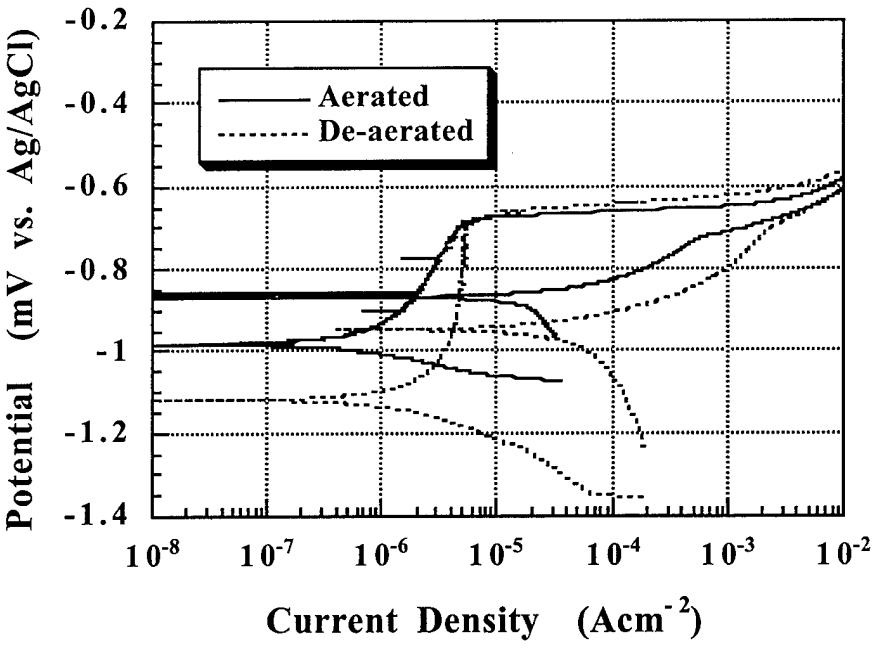

Fig. 6(b) CP scans for unreinforced Al6061-T6.

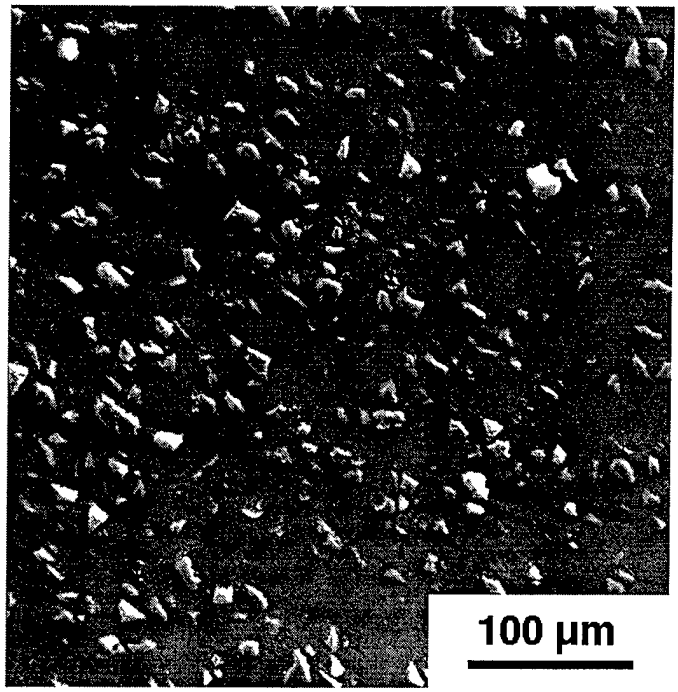

Fig. 7. SEM micrograph of Al_2O_3/Al6061-T4 MMC before immersion.

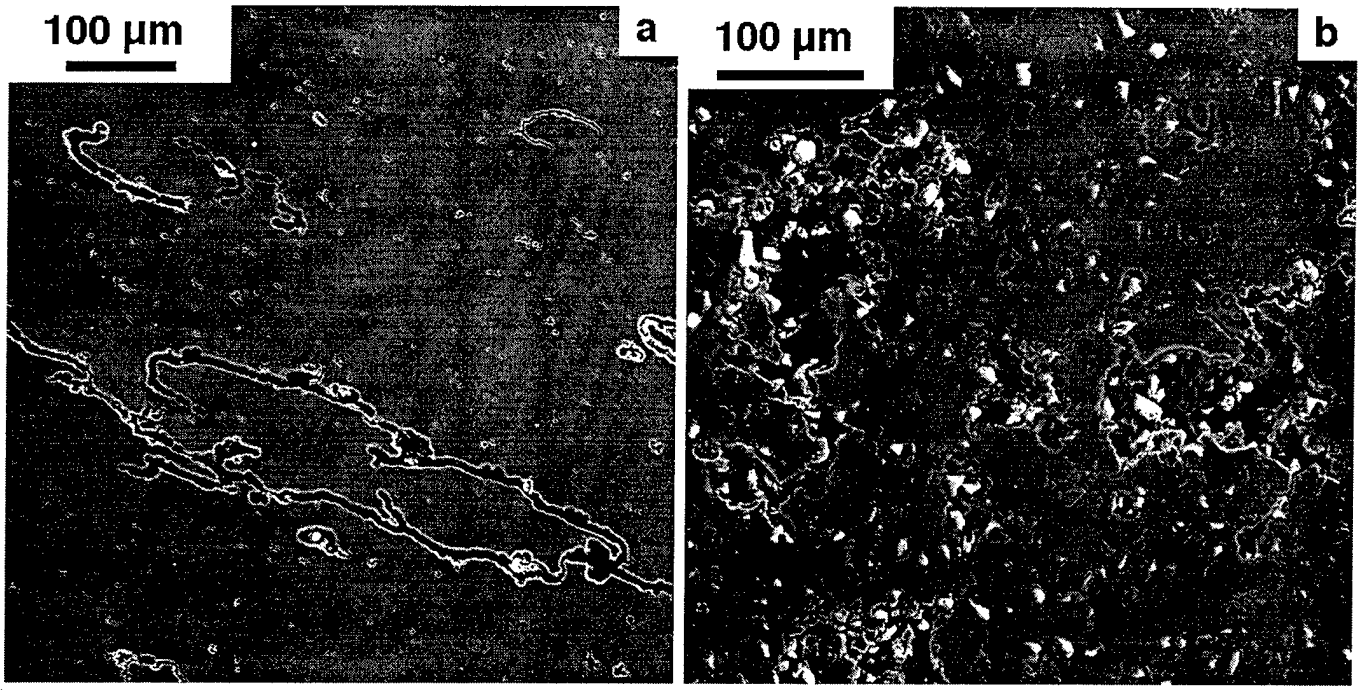

Fig. 8. SEM micrograph showing a) unreinforced alloy and b) T4 composite after 16 days immersion test.

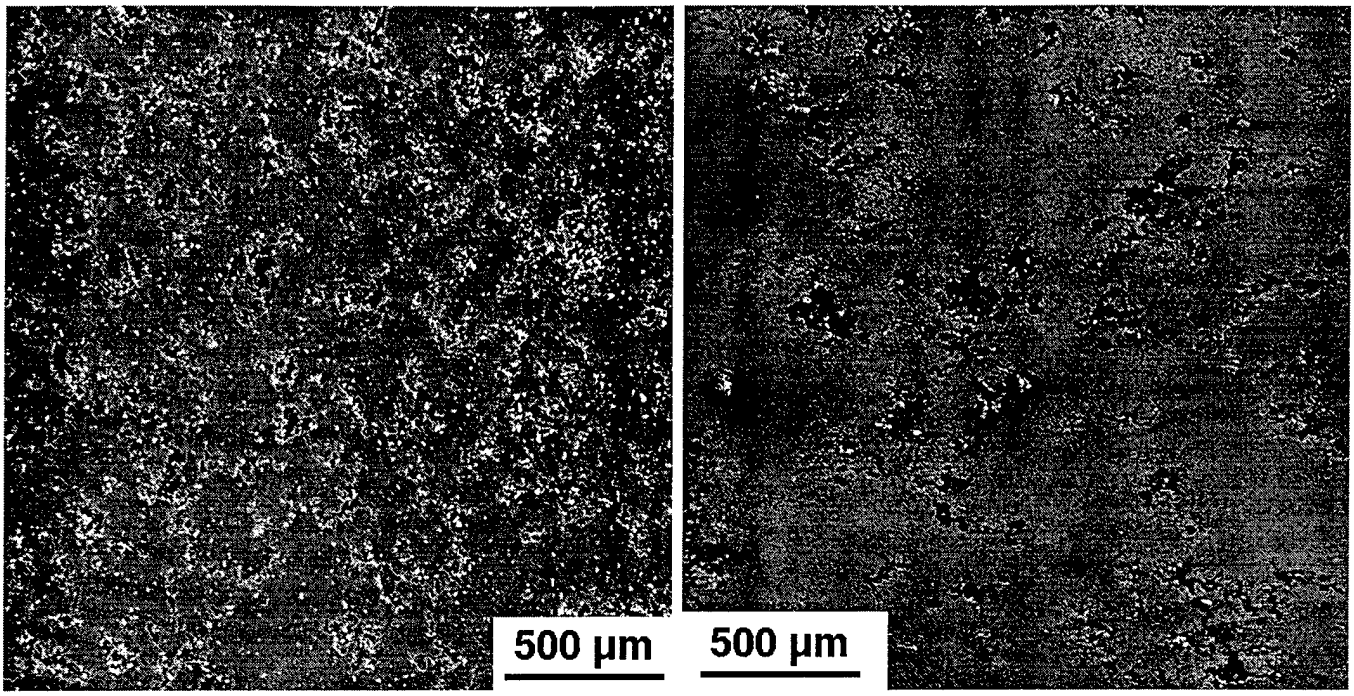

Fig. 9 Low magnification views of the extent of pitting in the Al_2O_3/6061-T4 MMC after (a) 8 days and (b) 16 days immersion.

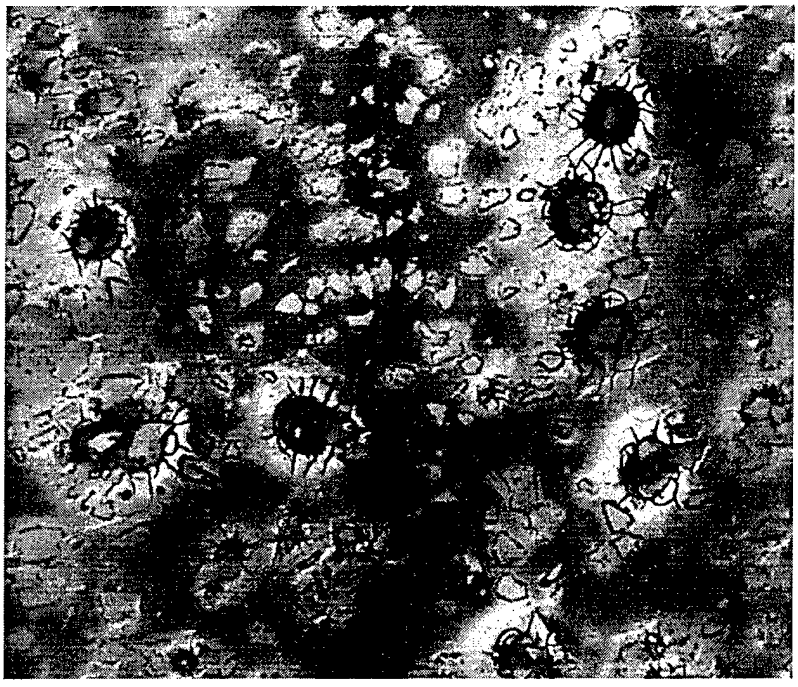

Fig. 9(c) Higher magnification of Fig. 9(b) before removal of corrosion product.

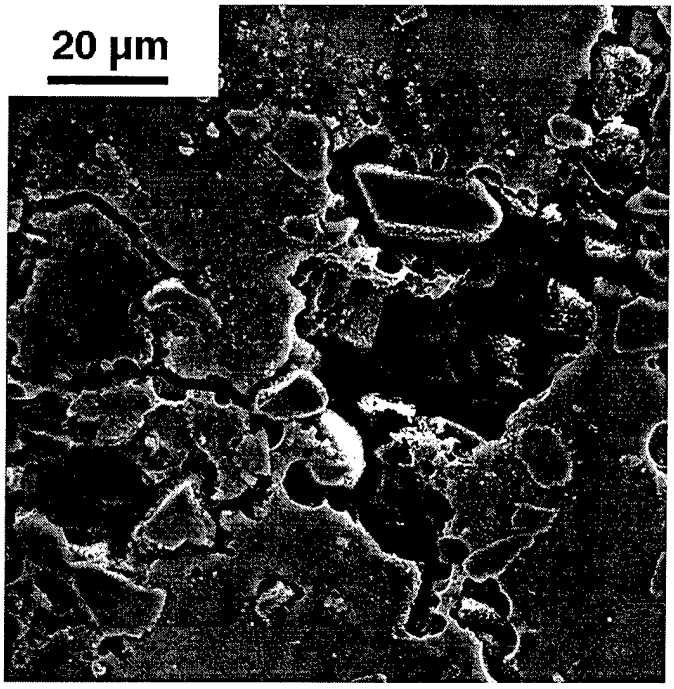

Fig. 10. Large pit at grain boundary in Al_2O_3/6061-T4 MMC after 8 days immersion.

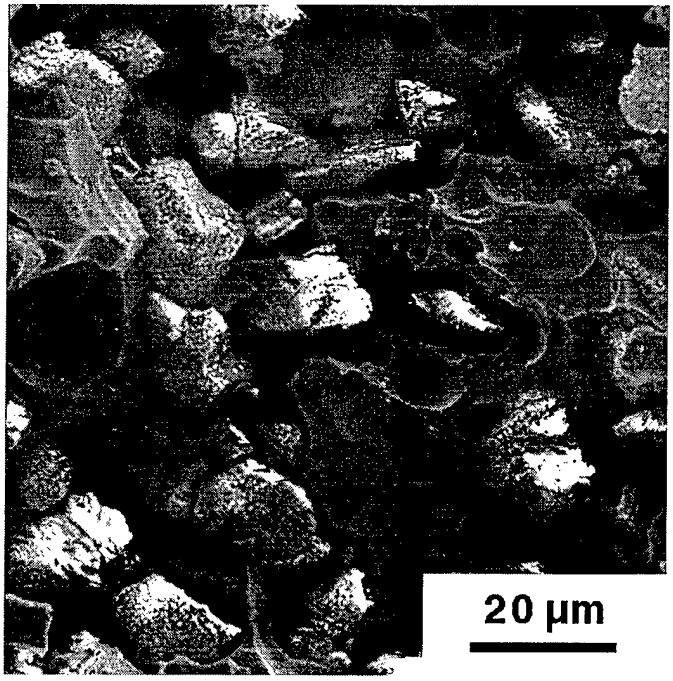

Fig. 11. High magnification view of pit interior showing particles remaining in cusp-shaped recesses.

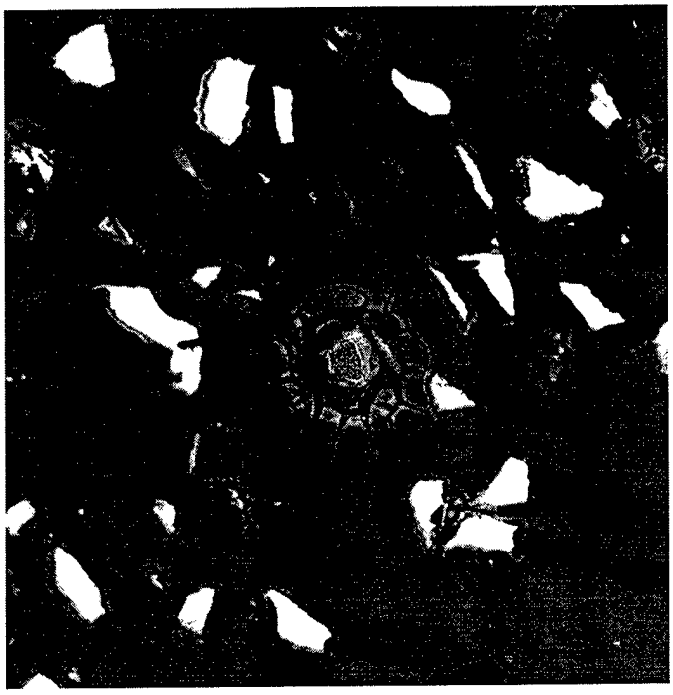

Fig. 12 Titanium-rich intermetallic particle showing rapid pit initiation after 30 minutes immersion while nearby Al_2O_3 particles remain unattacked.

Fig. 13. Microstructure of Al6061-T6 showing precipitation of Mg_2Si on the dislocation substructure.

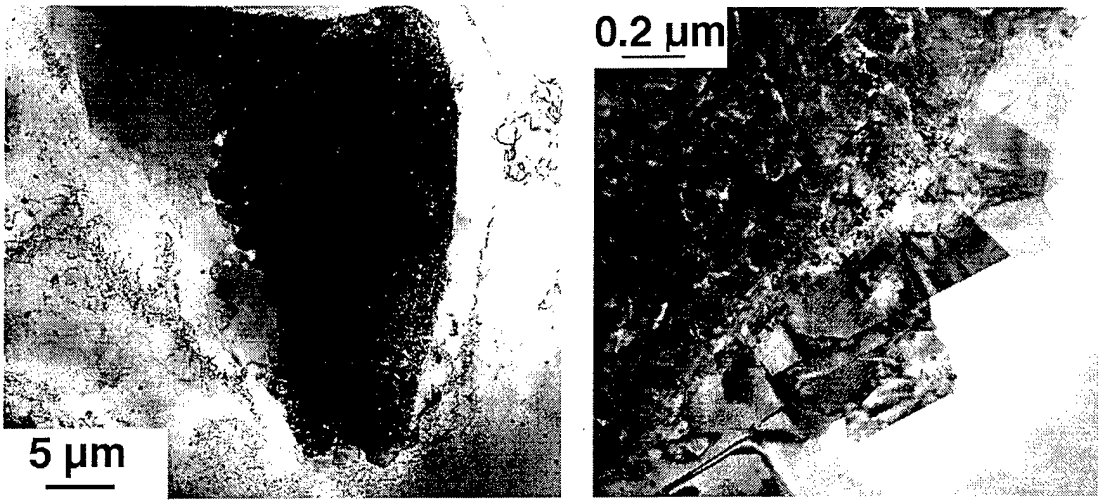

Fig. 14(a) Titanium-rich intermetallic particle (TEM micrograph). (b) high magnification view of particle edge

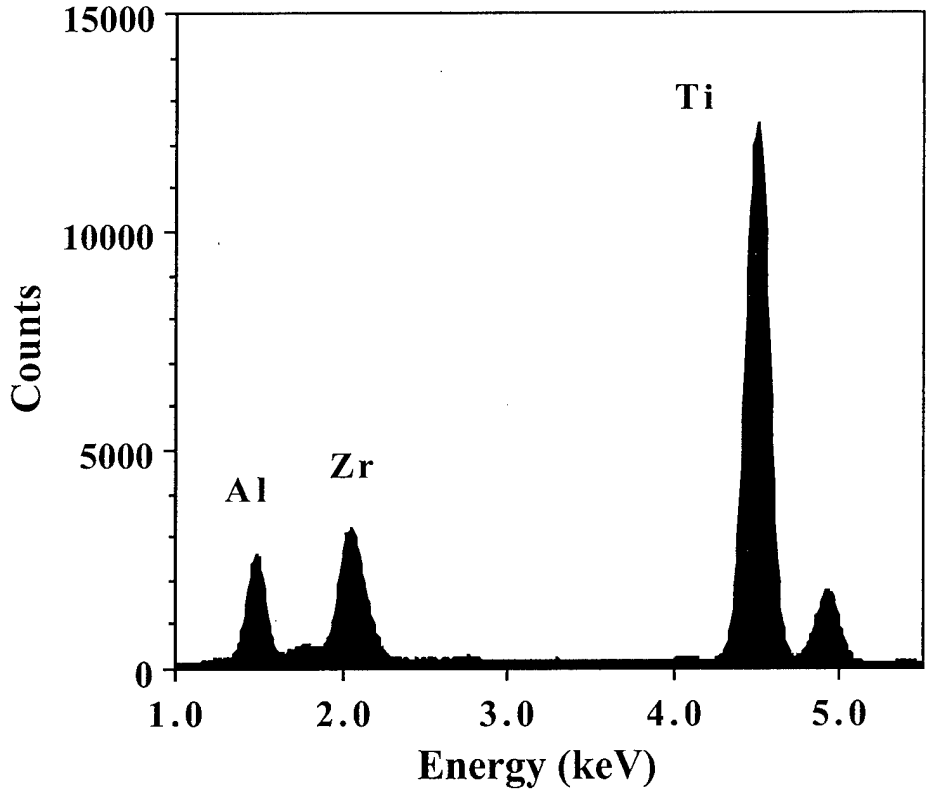

Fig. 14(c). EDS spectrum of the blocky particles of Fig. 14(b).

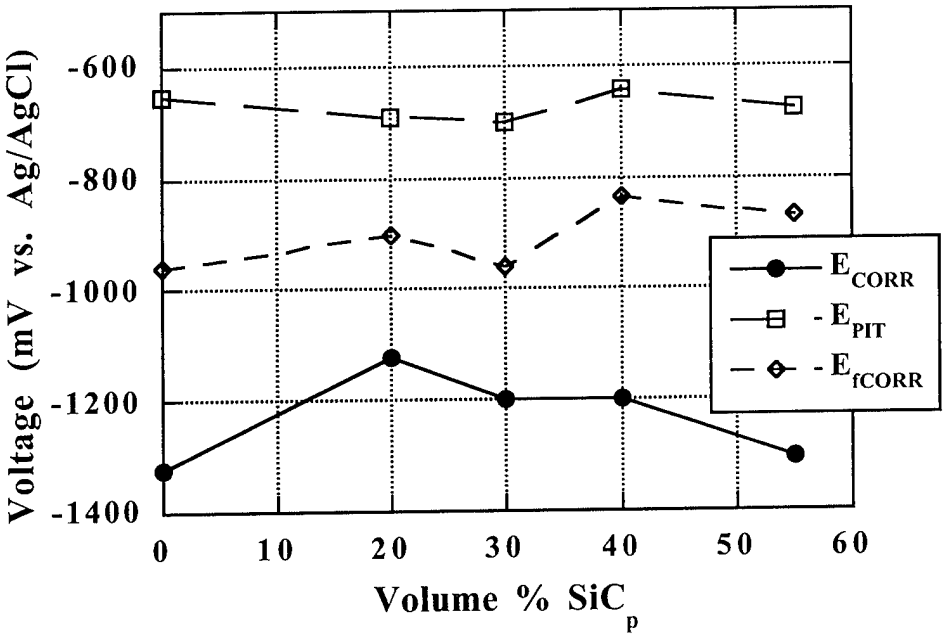

Fig. 15(a). Principal corrosion parameters in de-aerated solution as a function of V_f% SiC_p particles.

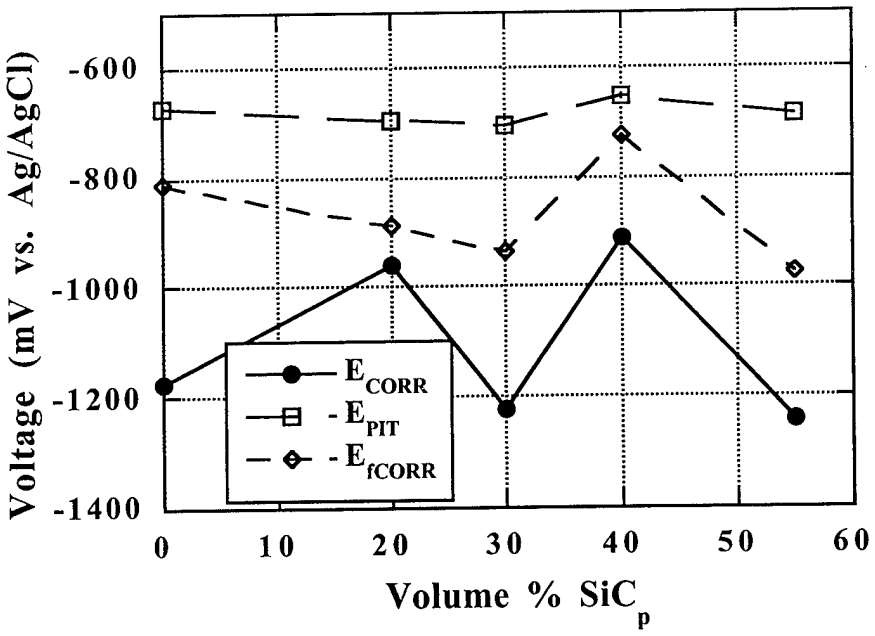

Fig. 15(b). Principal corrosion parameters in aerated solution as a function of V_f% SiC_p particles.

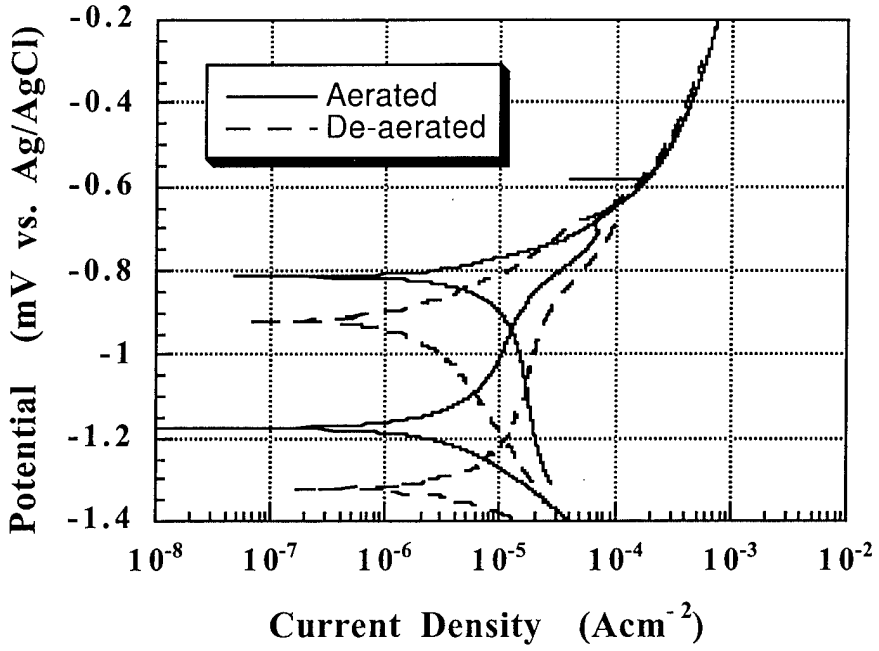

Fig. 16. Cyclic polarization scans of Al-10%Si unreinforced matrix alloy in aerated and de-aerated solutions.

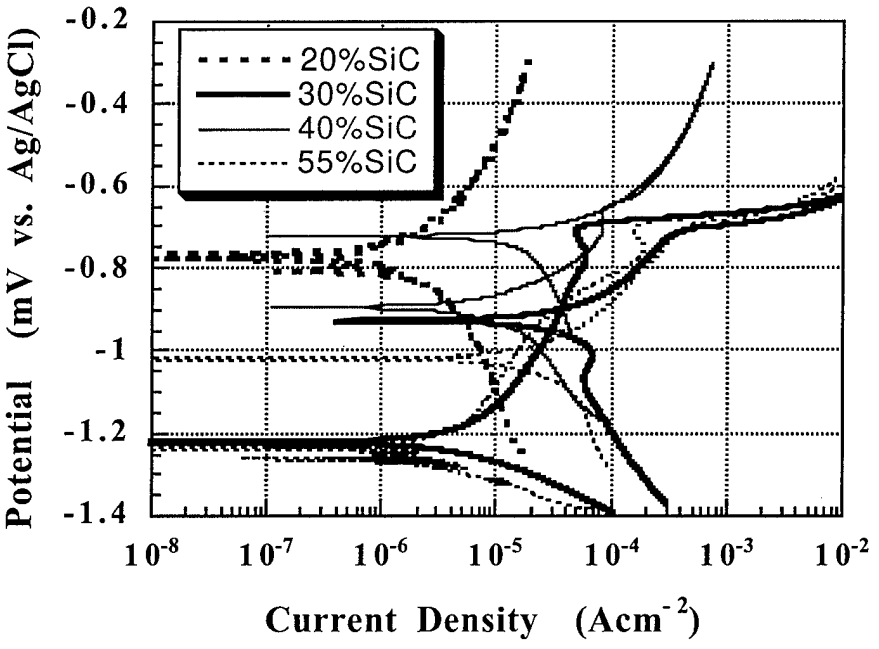

Fig. 17. Cyclic polarization scans for various V_f%SiC samples in aerated solution.

Fig. 18(a). Optical microstructure of unreinforced Al-Si alloy showing silicon eutectic.

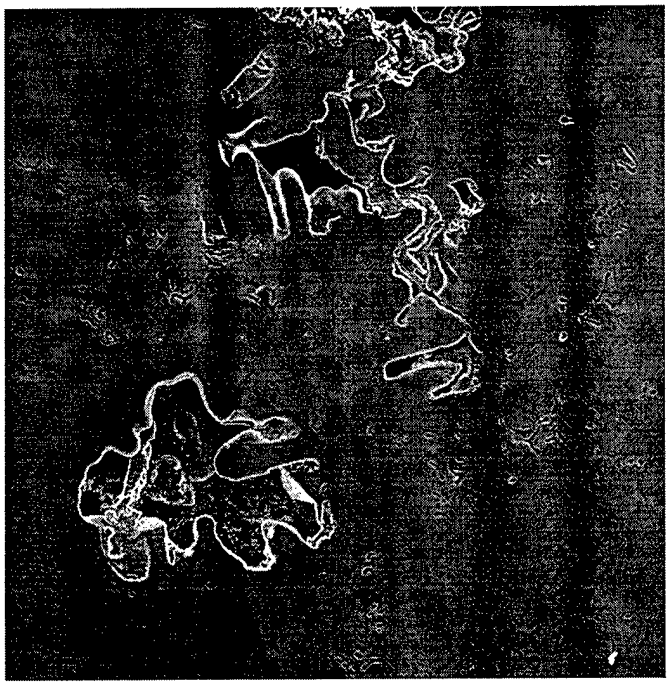

Fig. 18(b). SEM micrograph showing interdendritic shrinkage porosity.

Fig. 19. 0%SiC_p/Al-Si showing selective removal of one type of intermetallic particle during 12 day immersion test.

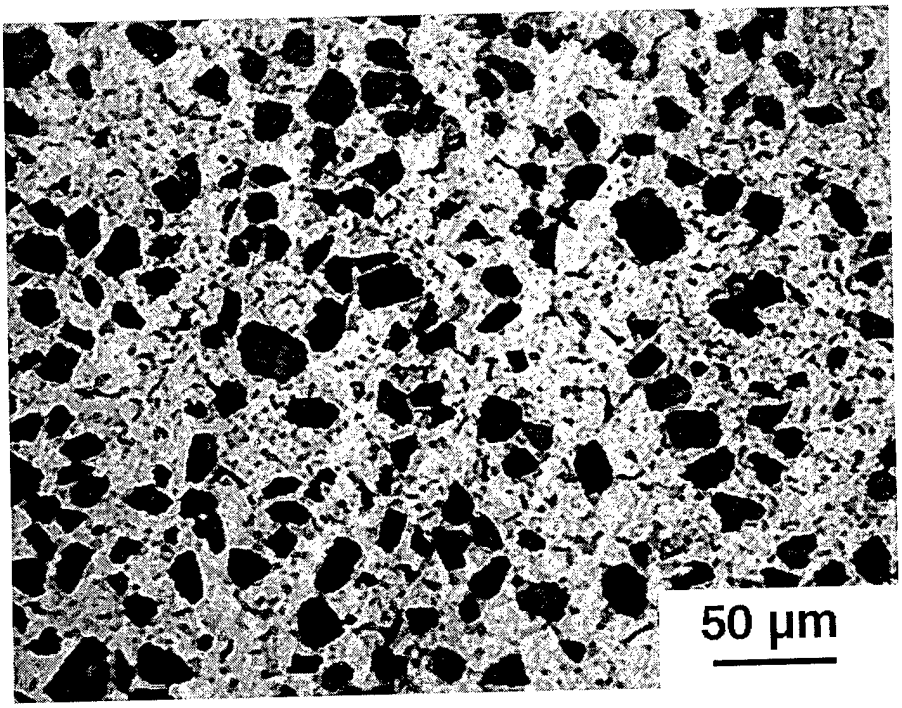

Fig. 20(a). 30%SiC_p showing particulates and Si eutectic at cell boundaries.

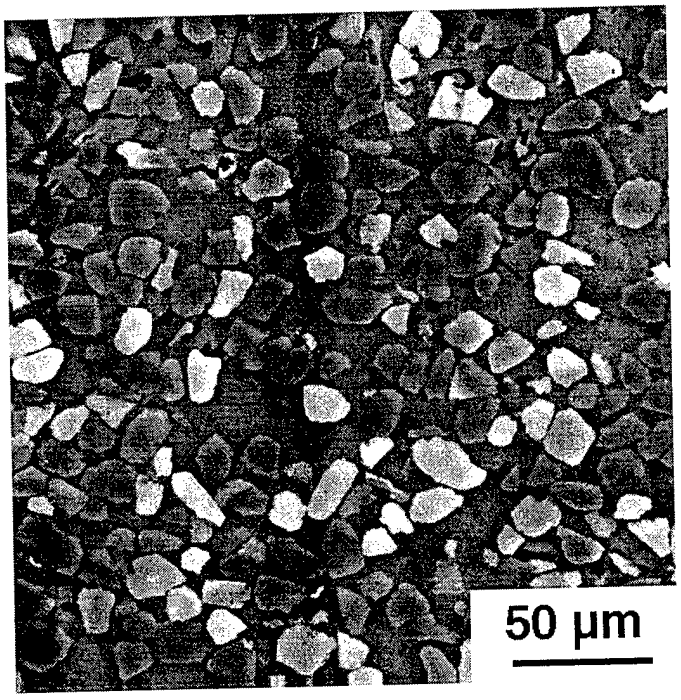

Fig. 20(b). SEM micrograph of 55%SiC_p/Al-Si showing uniform distribution of particles and microporosity.

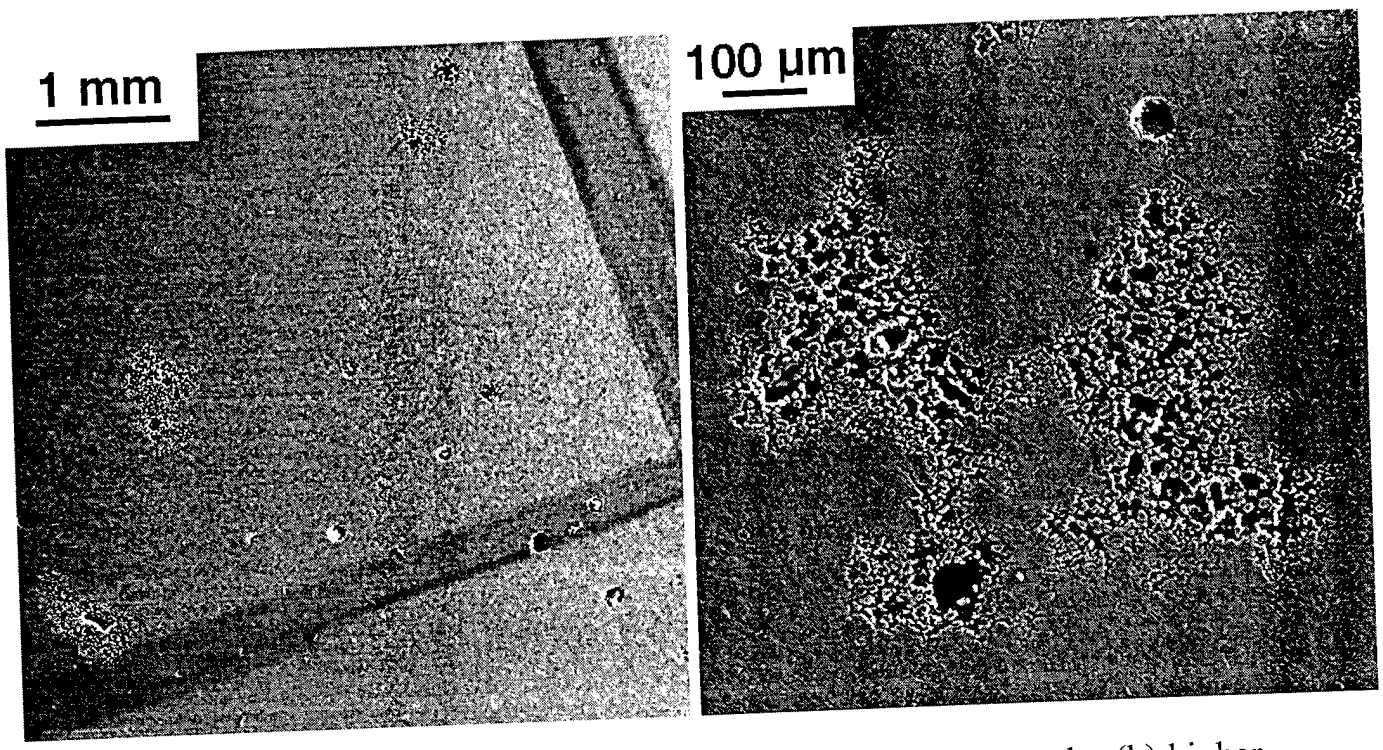

Fig. 21. (a) Low magnification SEM view showing localized attack. (b) higher magnification view of similar area.

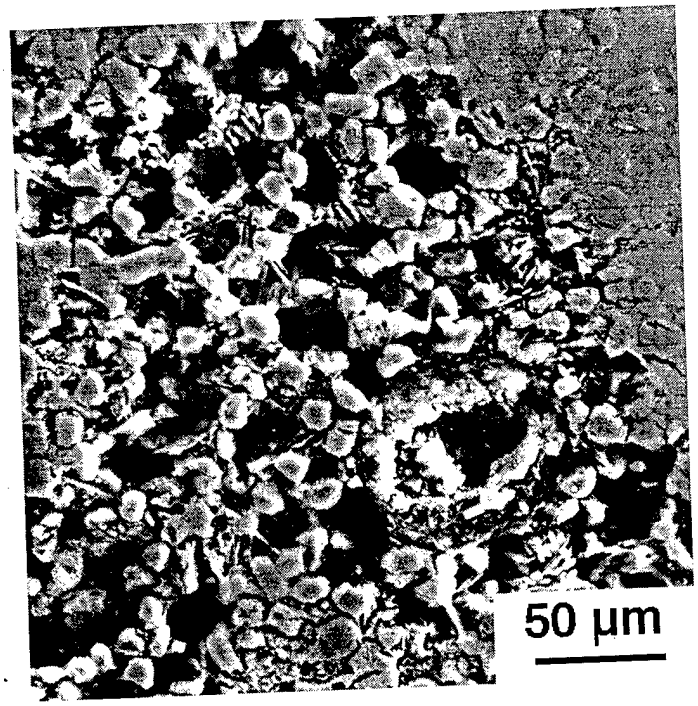

Fig. 21(c). 20%SiC_p after electrochemical testing showing progressive attack of Al matrix leaving exposed SiC and Si.

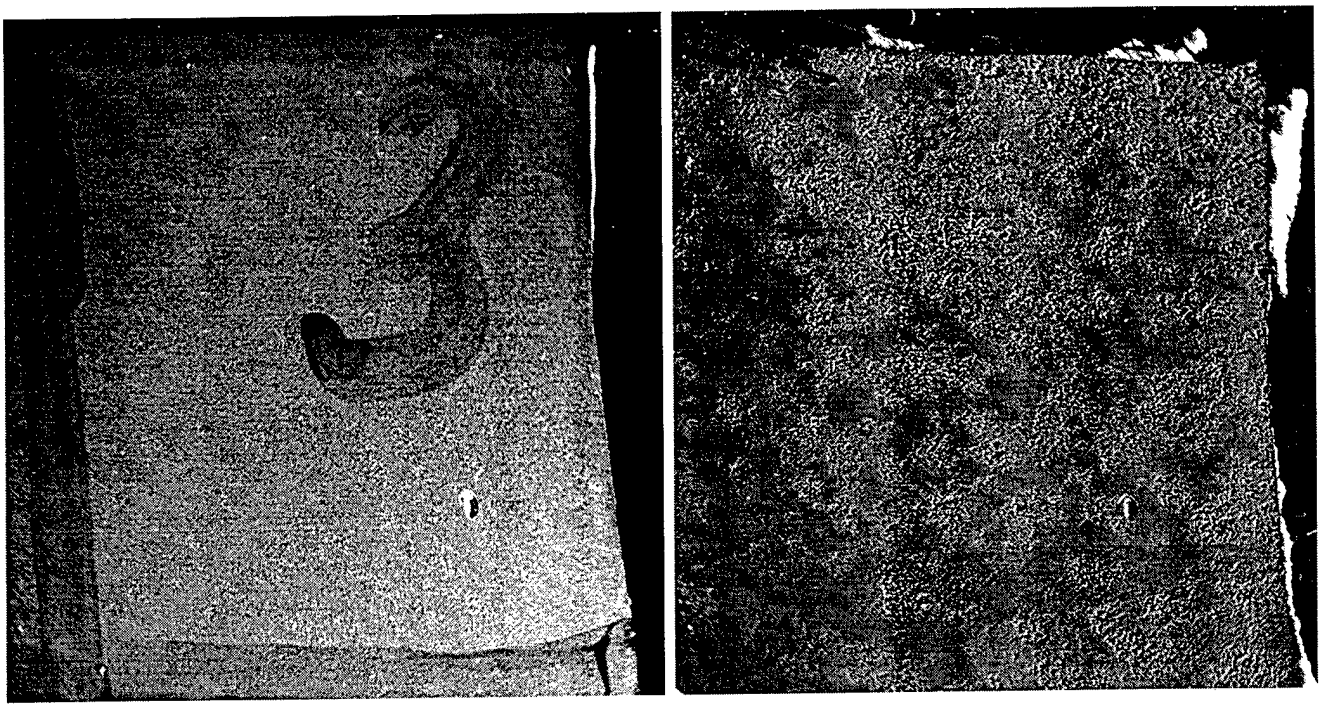

Fig. 22. (a) & (b) Same area of 30%SiC MMC before and after cathodic polarization testing showing severe corrosion.

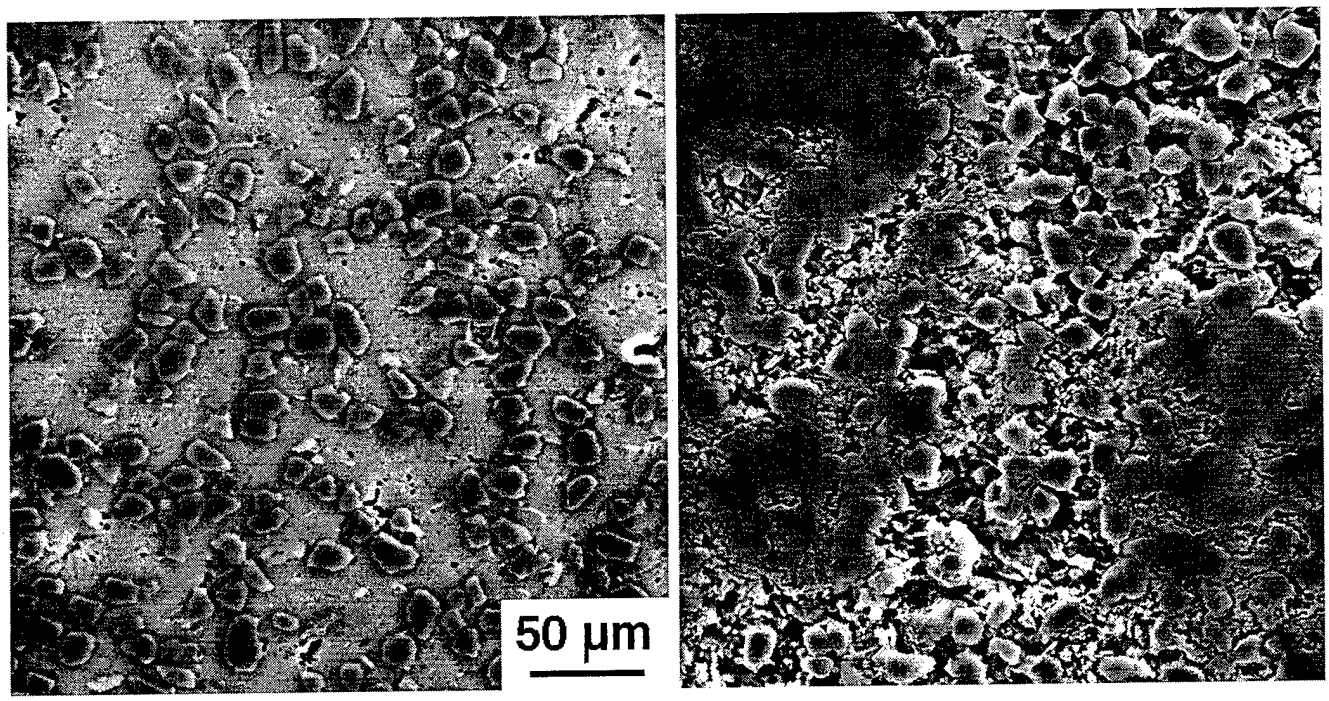

Figs. 23 30%SiC MMC (a) before and (b) after cathodic polarization test.

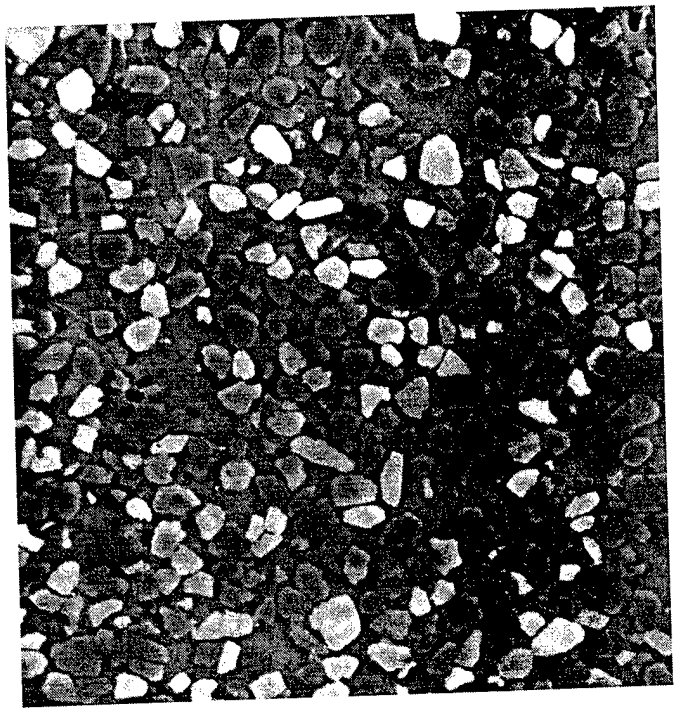

Fig. 24(a). 55%SiC MMC before electrochemical testing.

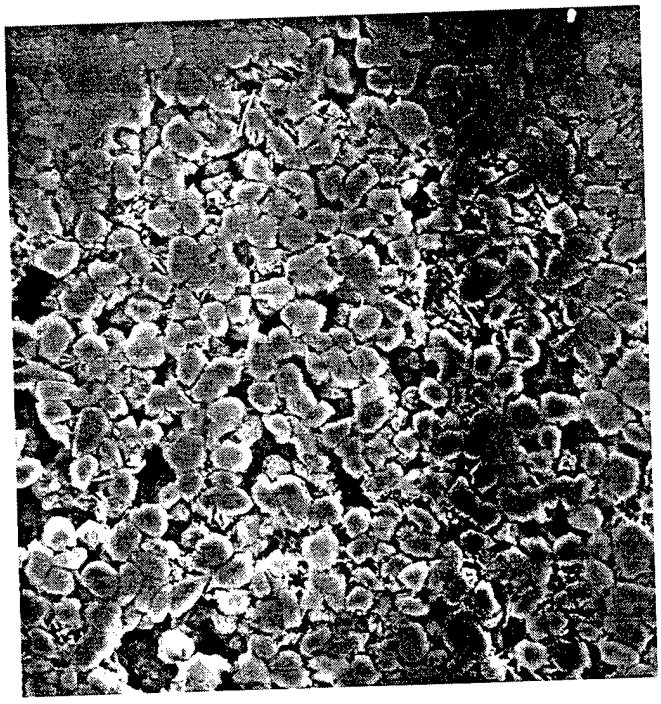

Fig. 24(b). 55%SiC MMC after electrochemical testing.